Freie Universität Berlin

ALFRED-WEGENER-INSTITUT
HELMHOLTZ-ZENTRUM FÜR POLAR-
UND MEERESFORSCHUNG

Characterizing thermo-erosional landforms in Siberian ice-rich permafrost

Morphometric investigations in the Lena Delta using high-resolution satellite imagery and digital elevation models

Master thesis

to attain the academic degree

Master of Science (M.Sc.) in Geography

Submitted by

Samuel Stettner

Institute for Geographical Science
Freie Universität Berlin

Berlin, November 2014

Samuel Stettner,

geboren am 18. Februar 1986 in Siegen

Addresse: Skalitzer Straße 81, D-10997, Berlin
Email: samuel.stettner@awi.de
Matrikelnummer: 4062919

Erstgutachter: **Prof. Dr. Karl Tilman Rost**   Zweitgutachterin: **Dr. Anne Morgenstern**
Adresse: Malteserstraße 74-100,   Adresse: Telegrafenberg A43
                 Haus G, D-12249 Berlin   D-14473 Potsdam
Email: tilman.rost@fu-berlin.de   Email: anne.morgenstern@awi.de

Contents

List of figures

List of tables

Kurzfassung

Die beschleunigte Erwärmung der Arktis infolge des Klimawandels führt zu einer weit-reichenden Degradation von Permafrost und wirkt sich auch auf die Stabilität arktischer Ökosysteme aus. Hierbei sind Thermokarst und Thermoerosion zwei prominente Prozesse der Permafrost Degradation. Die räumliche Verbreitung von thermo-erosiven Prozessen und den hieraus resultierenden Landformen (z.B. Gullys und Täler), sowie deren Einfluss auf die Permafrost Degradation sind noch unzureichend quantifiziert. Die vorliegende Arbeit widmet sich diesem Forschungsrückstand und nutzt eine Kombination aus Felddaten, hoch-auflösenden Satellitendaten, sowie digitalen Geländemodellen (DGMs) für eine detaillierte Inventarisierung und räumliche Analyse von Thermoerosionsformen, um deren Dynamik und Relevanz bei der Degradation von eisreichem Permafrost zu verstehen. Das Untersuchungs-gebiet im zentralen Lena Delta setzt sich zu großen Teilen aus eis- und organikreichen syngenetisch gefrorenen Sedimenten mit spät-pleistozänem Alter zusammen (Eis Komplex). Neben polygonaler Tundra, Thermokarst Seen, weiten Thermokarst Ebenen und ungestörtem Eis Komplex gibt es im Untersuchungsgebiet auch eine große Varietät von Thermoerosions-Tälern. Während einer Expedition im Sommer 2013 wurden mittels Ecktzeitkinematik-GPS 11 Kontrollpunkte, 28 topographische Quer-, sowie drei Längsprofile in drei repräsentativen Gebieten vermessen. Ein geometrisch konsistenter Datensatz aus GeoEye-1, RapidEye und ALOS PRISM Satellitendaten, sowie mehrere hochaufgelöste DGMs mit 5m Bodenauflösung wurden erstellt. Die DGMs wurden anhand der Felddaten hinsichtlich absoluter Höhe und Hangneigung evaluiert und das thermo-erosive Gewässernetzwerk auf Grundlage der Satellitendaten digital kartiert und morphometrisch analysiert. Die höchste DGM Genauigkeit wurde mit einer Kombination von sechs Stereopaaren der Jahre 2006 und 2009 erzielt und die aus dem DGM abgeleiteten Quer- und Längsprofile spiegeln die tatsächliche Form und Morphmometrie der Täler wieder. Das Fließgewässernetz zeigt innerhalb von weiten Thermokarstsenken einen hohen Grad an Organisation und ist auf den Eis Komplex Ober-flächen nur schwach entwickelt. Die Täler sind tendenziell nach dem Höhengradienten des Untersuchungsgebietes in Richtung Nordwest orientiert. Talabschnitte außerhalb von Thermokarstsenken zeigen jedoch zwei Hauptrichtungen, die das polygonale Netz im Unter-grund wiederspiegeln könnten. Einhergehend mit einer weiteren Erwärmung des Permafrosts infolge des Klimawandels werden Thermokarst und Thermo-Erosion wesentlich zur voranschreitenden Permafrost Degradation beitragen. In diesem Zusammenhang spielen die sich im Eis Komplex weiter ausbreitenden thermo-erosiven Gewässernetzwerke eine entscheidende Rolle bei dem Transport des durch Permafrost Degradation freigesetzten fossilen organischen Kohlenstoffs in das System der Laptev See.

Abstract

Rapid warming of the Arctic promotes widespread degradation of permafrost and affects the stability of arctic ecosystems. Thermokarst and thermal erosion are two major processes of permafrost degradation. The spatial extent of thermo-erosional processes and related landforms (e.g. gullies and valleys) and their impact on the widespread degradation of permafrost remains not well quantified. Addressing this research gap, this study is using a combination of field data, high-resolution satellite data and photogrammetically derived digital elevation models (DEMs) to conduct a detailed inventory and spatial analysis of thermo-erosional landforms in order to understand their dynamics as well as their relevance for permafrost degradation. The study area in the central Lena Delta is mainly composed of ice- and organic-rich and syngenetically frozen deposits of Late Pleistocene age called Ice Complex. Besides polygonal tundra, thermokarst lakes, wide thermokarst depressions and undisturbed Ice Complex surfaces the study area features a broad variety of thermo-erosional valleys. During an expedition in summer 2013 RTK GPS measurements of 11 ground control points and 28 transversal and 4 longitudinal profiles were conducted in three key sites. Geometric data fusion of GeoEye-1, RapidEye and ALOS PRISM datasets was performed and several high-resolution DEMs were generated. The DEMs were evaluated for absolute height and slope against the field dataset and the thermo-erosional stream network was mapped and morphometric analysis of the identified features was performed. The highest DEM accuracy was achieved when using a combination of six stereopairs from the years 2006 and 2009. The DEM derived transversal and longitudinal profiles reflect the actual shape and morphometry of the valleys. The identified stream network shows levels of high organization within thermokarst depressions and is poorly developed on the Ice Complex surface. The stream orientation tends to follow the height gradient of the study area towards northwest, while streams outside of thermokarst depression show two main directions that could reflect the polygonal network in the ground. Accompanying permafrost warming thermokarst and thermo-erosional activity will further promote permafrost degradation. In this context thermo-erosional stream networks will expand within the Ice Complex and act as a major agent for the transport of remobilized fossil organic carbon to the Laptev Sea system.

1 Introduction

The Arctic is a substantial and very sensitive element in the Earth's climate system that is undergoing rapid and far reaching changes. The last decades in the Arctic are characterized by significant warming due to climate change. These changes occur about two times faster than the global average [*AMAP*, 2011] and have a significant impact on polar permafrost regions. As a consequence permafrost thermal state is affected by rising temperatures and resulting permafrost degradation is leading to fundamental landscape changes as observed throughout the northern latitudes [*AMAP*, 2011; *Romanovsky et al.*, 2010b]. Within the frozen deposits of northern permafrost regions 1762 Pg of carbon is stored, about twice as much as is present in today's atmosphere [*Tarnocai et al.*, 2009]. This ancient carbon pool is very sensitive to temperature changes and can potentially be mobilized through thawing [*McGuire et al.*, 2009; *Schuur et al.*, 2008]. When released into the atmosphere these carbon stocks could further accelerate global warming resulting in a positive feedback mechanism [*Koven et al.*, 2011].

In periglacial environments, thermokarst and thermal erosion are two major processes of permafrost degradation that form prominent landscape features in Arctic lowlands. While thermokarst is defined as a process by which characteristic landforms result from the thawing of ice-rich permafrost or the melting of massive ice, thermal erosion is the erosion of ice-bearing permafrost by the combined thermal and mechanical action of moving water [*van Everdingen*, 2005]. This process is leading to the erosion of ice-bearing coastlines [*Günther et al.*, 2013], shores of lakes with significant wave activity [*Jones et al.*, 2011], riverbanks [*Costard et al.*, 2007] and land surfaces [*Morgenstern*, 2012]. Thermokarst and thermo-erosional processes not only contribute to the release of fossil organic matter to the atmosphere [*Schuur et al.*, 2009], but substantially alter the water and energy balances of the affected ecosystems and consequently change the living conditions of arctic communities.

While thermokarst-related processes and resulting landscape features have been well studied in Siberian ice-rich permafrost regions [*Grosse et al.*, 2007; *Günther*, 2009; *Morgenstern et al.*, 2013; *Ulrich et al.*, 2010], few detailed investigations have been undertaken regarding thermo-erosional processes, the resulting features and their relevance for permafrost degradation. Thermo-erosional valleys in the Lena River Delta have been described by *Grigoriev* [1993]. In the context of an overall quantification of thermokarst-affected terrain types in two regions of the East Siberian, thermo-erosional valleys were mapped by *Grosse et al.* [2006]. *Morgenstern* [2012] conducted a detailed inventory of thermo-erosional landforms for three ice-rich arctic lowland sites in Siberia based on Landsat imagery and revealed substantial differences in the drainage networks that depend on

previous degradation by thermokarst, neo-tectonics and the general hydrological and relief situation. On Bylot Island in the Canadian Arctic, rapid formation of thermo-erosional gullies and the development of subsurface channels are reported [*Fortier et al.*, 2007; *Godin et al.*, 2014]. The impacts of thermal erosion on the local environment are diverse and include: the erosion of ice-rich sediments; alteration of sediment; nutrient and carbon transport to rivers, lakes and the sea; the restructuring of drainage networks; changing of stream runoff volumes and their timing; and the drainage of thermokarst lakes [*Rowland et al.*, 2010]. Thus, the understanding of thermo-erosional processes in the context of climate change and the wide-spread degradation of permafrost landscapes is of major importance.

For the morphometric analysis of thermo-erosional features (e.g. channels, gullies, valleys) and their surrounding terrain, high resolution Digital Elevation Models (DEM) are fundamental. Operational remote sensing elevation products that are available for arctic regions are delivered with a medium to coarse resolution that is insufficient for detailed morphometric studies. Therefore, the use of photogrammetric techniques to extract high-resolution DEMs from stereoscopic remote sensing datasets is a common and useful approach [*Wilson*, 2012]. However, photogrammetric DEM generation in low-contrast arctic tundra environments with low height gradients is challenging and time consuming, and DEM products must carefully be validated [*Kääb*, 2008]. Therefore, extensive field-work and ground truthing is essential to perform multi-platform and multi-temporal image fusion, and to control the quality of the derived products.

This study aims at closing research gaps regarding the degradation of ice rich permafrost in Siberian arctic lowlands by thermal erosion. This will be done by performing morphometric analyses by using a combination of field and remote sensing data and high-resolution DEMs.

The following research questions are formulated:

- Are DEMs extracted from ALOS-PRISM satellite data a suitable basis for the morpho-metric analysis of thermo-erosional valleys in ice-rich permafrost?
- How are thermo-erosional valleys distributed in the study area?
- What are the driving factors for the presence of the identified valley types?

Based on the research questions the main objectives are:

- To generate high-resolution DEM products
- To evaluate the ALOS-PRISM DEM for the morphometric parameters elevation and slope.
- To map and characterize thermo-erosional landforms.
- To identify the driving factors for the development of these landforms.

2 Scientific background

2.1 Permafrost

Permafrost is defined as "ground (soil or rock and included ice and organic material), that remains at or below 0°C for at least two consecutive years" *van Everdingen* [2005]. According to this definition, permafrost regions make up ca. 24 % of the land area of the Northern Hemisphere [*Zhang et al.*, 2008]. In Russia, more than half of the landmass is underlain by permafrost, thus it is one of the world largest permafrost regions [*Romanovsky et al.*, 2010a] (Figure 2-1). The periglacial extent not only includes high latitude landscapes, but also vast areas of the continental shelves of the Arctic Ocean and mountainous areas in lower latitudes [*Romanovsky et al.*, 2010b] (Figure 2-1).

The most important environmental drivers of permafrost conditions are topographic features (e.g. relief and aspect), snow cover, vegetation, subsurface material and the moisture content of the ground [*French*, 2007; *Washburn*, 1979].
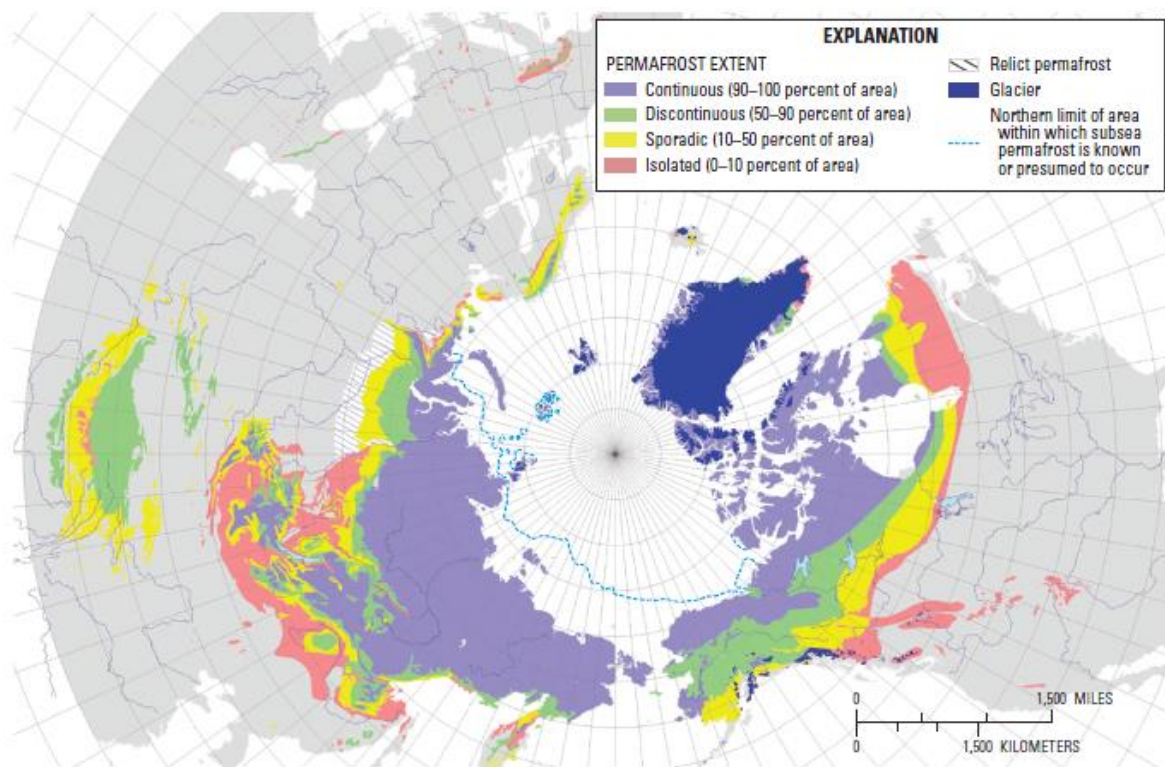
Figure 2-1: Permafrost extent in the Northern Hemisphere; after *Brown et al.* [1997] in *Heginbottom et al.* [2012].

Four major regions of permafrost distribution can be distinguished (Figure 2-1 and Figure 2-2):

1. Within the *continuous zone* 90 to 100 % of the area is underlain by permafrost. It is mostly found in the high latitudes of the Northern Hemisphere, with climate conditions that favor active formation of frozen ground (ca. -15°C mean annual air temperature). Most continuous permafrost was formed during or before the last glacial period.

2. In the *discontinuous zone* permafrost covers 50 to 90 % and is separated by taliks.

3. Within the *sporadic zone* permafrost covers an area of 10 to 50 %. It is often relict and in the process of degradation, or it is much younger and formed within the last several thousand years.

4. The *isolated zone* shows only single patches of frozen ground in an otherwise unfrozen area and covers <10 % of the total area. This zone is a result of advanced permafrost degradation [*French*, 2007; *Romanovsky et al.*, 2010b; *Weise*, 1983].
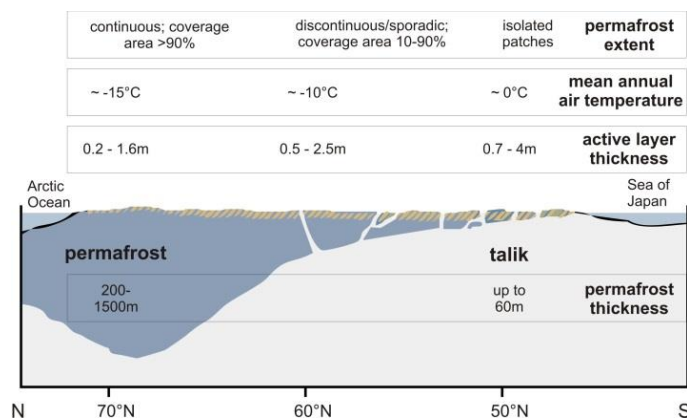
Figure 2-2: Transect of the permafrost zone of East Siberia, after *French* [2007]

Permafrost is overlain by an active layer (Figure 2-3), which is affected by seasonal freeze and thaw cycles. The depth of the active layer can vary significantly from year to year as well as between locations. It is strongly connected to the permafrost controlling factors listed above. The permafrost table is the boundary between the active layer and the upper limit of the permafrost (Figure 2-3) [*Washburn*, 1979].

The most important factor for the temperature regime of the active layer is the vegetation cover with its isolating properties. Furthermore exposition, topography and sediment type influence the thickness of the active layer. While active layer thicknesses of up to 3 m can be observed in subarctic regions or areas with coarse grained sediments, just several centimeters of thawing occur in high arctic regions.
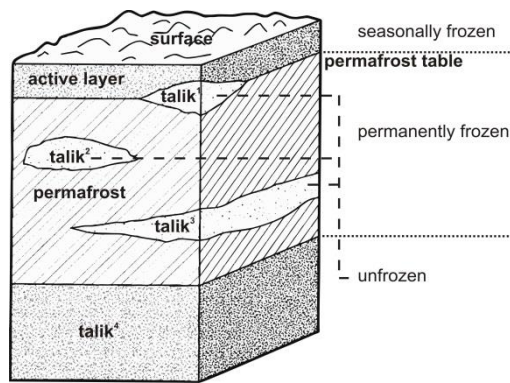
Figure 2-3: Vertical differentiation of the permafrost zone; talik[1]: suprapermafrost; talik[2]: closed; talik[3]: intrapermafrost; talik[4]: subpermafrost; after French [2007], modified by *Strauss* [2010].

2.2   Ground ice

Ground ice is a main feature of permafrost and refers to all types of ice contained in freezing and frozen grounds [*van Everdingen*, 2005]. The stability of landscapes containing frozen soils is strongly connected to the ground ice content and the degradation of permafrost would mean a loss in system stability [*Romanovsky et al.*, 2007].

According to *Mackay* [1972] ground ice can be classified into four types: 1) pore ice, 2) segregated ice, 3) vein ice and 4) intrusive ice. Particularly important for this research is a type of vein ice called ice wedges (Figure 2-4 and Figure 2-5). Due to a rapid temperature drop in the winter, the ground can shrink and crack. In late May or early June, melt water from snow then trickles down into the cracks and forms thin veinlets of ice. Through repeated cracking at the same place the ice wedge grows from year to year [*Lachenbruch*, 1963; *Mackay*, 1990] (Figure 2-5).
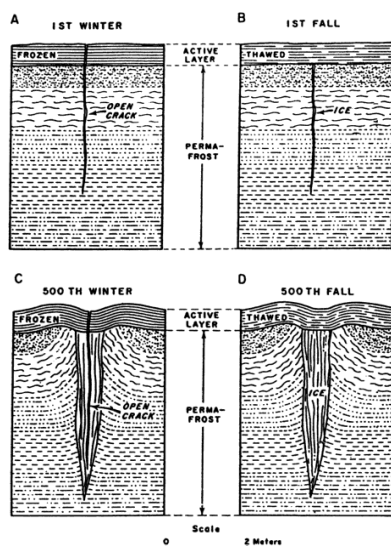
Figure 2-4: Scheme of the evolution of an ice wedge according to the contraction cracks [Lachenbruch, 1963]
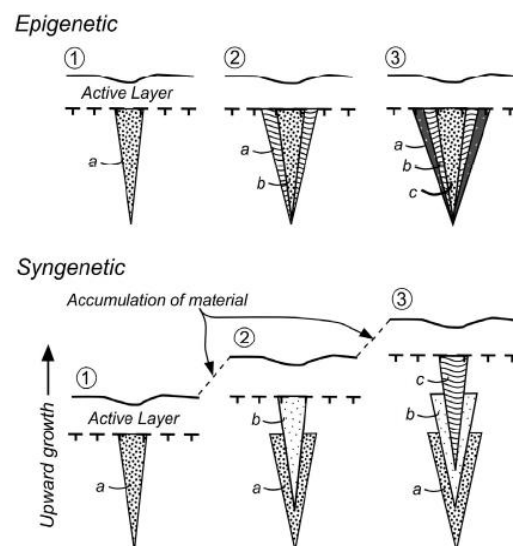
Figure 2-5: Schematic diagram showing the growth of epigenetic and syngenetic ice wedges; point in time: (1) first, (2) second, (3) third; ice wedge at (a) first (b) second (c) third point in time [*Mackay*, 1990].

Syngenetic ice wedges form at approximately the same time as the enclosing sediments accumulate, whereas epigenetic ice wedges form after sediment deposition [*French*, 2007] (Figure 2-5). Ice wedges originate through thermally induced cracking of the frozen groundand form under stable climatic conditions. Therefore simply their existence allows paleoclimatic interpretations [*Washburn*, 1979].

2.3   Polygonal nets and lakes

Ice wedges can form polygonal net features on the ground surface (Figure 2-6). These are characteristic for arctic tundra regions and widespread in the Lena Delta region [*French*, 2007] (Figure 2-7). There are two main types of ice wedge polygons: 1) low-center polygons and 2) high-center polygons. In low-center polygons the rim is usually higher than the center and ponds are developing inside (Figure 2-7).

The degradation of the polygon rims and changes in the hydrological regime can transform low-center polygons to high-center polygons, which are often accompanied by stream incision along the lines of the bordering ice wedges, interpolygon ponds and thaw lakes. While low-center polygons indicate a wet or poorly drained tundra environment, high-center polygons are mainly a feature of a dry tundra [*French*, 2007].
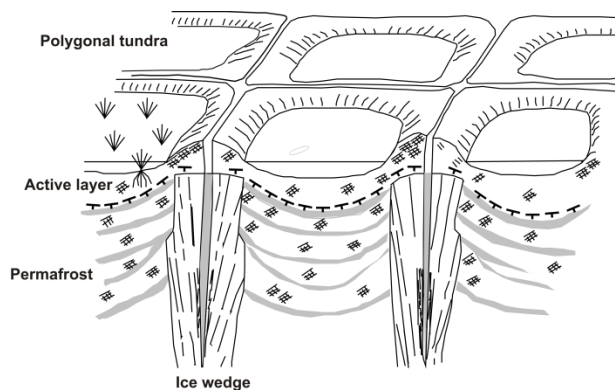
Figure 2-6: Schematic view of modern polygonal nets. After *Romanovskii* [1977], modified by *Strauss* [2010]

Figure 2-7: Polygonal tundra with polygon ponds in the Lena Delta

2.4   Ice Complex and Yedoma

Ice-rich and syngenetically frozen deposits of Late Pleistocene age are often referred to as "Ice Complex" [*Schirrmeister et al.*, 2012]. Ice Complex is exposed at shores and riverbanks by up to 50 m high outcrops composed of more or less degraded ice wedge bodies with thermokarst mounds in between (Figure 2-8). These exposed outcrops vertically or diagonally cut the polygonal ice wedge systems. Ice Complex deposits contain ice wedges which make up to 80 % of the total volume [*Schirrmeister et al.*, 2011].

Figure 2-8: Exposed Ice Complex sequence at the eastern shore of Kurungnakh Island, Lena Delta 2013.

Originally, "Yedoma" defines relief features in East Siberian lowlands, for instance elevated areas dissected by thermokarst depressions. Due to this striking relief feature, the native Yakutian people called it "Yedoma", which means "corroded earth" [*Tomirdiaro*, 1982]. Nowadays Yedoma is regarded as a morphological unit consisting of hills that are dissected by alas depressions. It is suggested that the Yedoma hills are remnants of former accumulation plains [*Romanovsky et al.*, 2010a]. In this work the term Ice Complex is used for this stratigraphic unit.

With regard to climate change, it is predicted that the Ice Complex deposits will be transformed from a long-term carbon sink to a major carbon source as these organic-rich sediments thaw and greenhouse gases are subsequently released [*Walter et al.*, 2006; *Zimov et al.*, 2006].

2.5   Permafrost degradation

2.5.1   Thermokarst and alasses

Thermokarst is a main process of permafrost degradation that forms characteristic landforms due to surface subsidence caused by the disturbance of the permafrost's thermal equilibrium. Climate change, disturbance of vegetation cover, fire, the shift of drainage channels or human activities can initiate thermokarst activity [*French*, 2007; *Washburn*, 1979].

As a result the active layer depth is increased and permafrost thaws beyond seasonal cycles. The volume loss of thawing ground ice can lead to the formation of thermokarst depressions, which are often called alasses in Siberia. In the Yakutian language an alas is a grassy, treeless meadow that occupies a flat-floored thermokarst depression with steep sides [*Tomirdiaro*, 1982]. Alasses are round to oval and many contain shallow lakes [*Washburn*, 1979]. The vertical dimension of alasses can be up to 40 m depth. Horizontally they can range

from 100 m to a few kilometers in diameter when adjacent alasses coalesce and form wide alas valleys (Figure 2-9; Stage 4a) [*Washburn*, 1979].
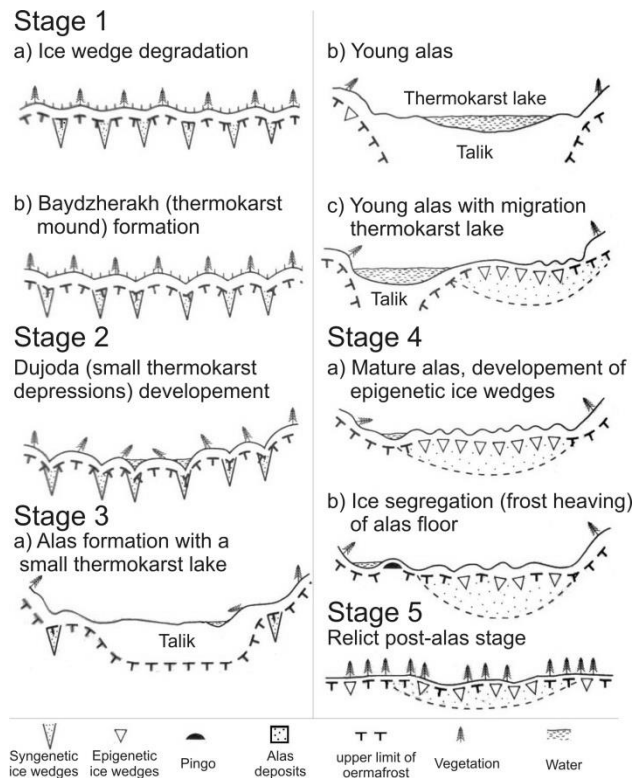
Figure 2-9: Stages of alas relief development in Central Yakutia; after *Soloviev* [1973], in *French* [2007].

2.5.2   Thermal erosion and thermo-erosional valleys

Thermal erosion is "The erosion of ice-bearing permafrost by the combined thermal and mechanical action of moving water" [van Everdingen, 2005].

Unlike thermokarst activity, where the eroded sediments stay at the same location, the process of thermal erosion includes the transport of the thawed sediments. This process occurs at sea coasts promoting coastal erosion [*Günther et al.*, 2013; *Lantuit et al.*, 2011], along riverbanks resulting in the shifting of islands [*Costard et al.*, 2003], and on surfaces of ice-rich sediments where it causes the rapid formation of thermo-erosional gullies and valleys [*Godin et al.*, 2014; *Morgenstern*, 2012]. Still, in today's understanding of periglacial geomorphology the link between slope form and process is still unclear; distinguishing between past and present processes is a major problem because many periglacial landscapes are in disequilibrium with current cold-climate conditions [*French*, 2007].

According to *Morgenstern et al.* [2014] eight different categories of thermo-erosional valleys can be distinguished for Siberian Ice Complex study sites (Table 2-1).

Table 2-1: Types of thermo-erosional valleys in Siberian ice-rich permafrost according to *Morgenstern et al.* [2014]

	Category	Occurrence	Characteristics	Hydrologic regime
a)	Short, straight gullies	On alas and thermo-karst lake slopes	Radially arranged around lakes and alasses; v- to u-shaped; steep gradient; up to few meters deep and wide; dense, fresh vegetation	Intermittent streams
b)	Drainage pathways in alasses	On alas floor	Connect residual and secondary thermo-karst lakes in partly drained alasses with the stream network outside the alasses; slightly intented into the alas floor; low gradient; up to a few meters wide; dense, vital vegetation	Intermittent and small permanent streams
c)	V-shaped ravines	Along steep coasts and cliffs; often due to lake drainage	V-shaped; steep to moderate gradient, up to tens of meters deep and wide; vegetation cover on floor and lower slopes often disturbed	Intermittent streams
d)	V-shaped valleys	In upper parts of the watersheds on Ice Complex surfaces	Mostly tributary valleys; v-shaped; moderate to low gradient, up to tens of meters deep and hundreds of meters wide; intact vegetation cover	Streams
e)	U-shaped valleys	On Ice Complex surface	U-shaped; low gradient, up to tens of meters deep and several to tens of meters wide; flat valley floor with vital vegetation	Intermittent and small permanent streams
f)	U-shaped valleys of permanent streams and rivers	Lower parts of long streams close to their mouth	U-shaped; low gradient, up to tens of meters deep and hundreds of meters wide; broad floors with distinct floodplains; often bare sediment exposed; oxbow and small thermo-karst lakes	Permanent, meandering streams
g)	Broad valley floodplains	Lower parts of long streams close to their mouth	Low gradient, up to tens of meters deep and hundreds of meters to kilometers wide; broad floors with distinct floodplains; often bare sediment exposed; oxbow and small thermokarst lakes	Permanent, meandering streams
h)	Water tracks	On gently sloping Ice Complex surfaces; on large, slightly inclined alas floors	Arranged in parallel; low gradient; not or only slightly indented into the surface; dense, vital vegetation	Poorly developed runoff systems

3 Study area and regional setting

The Lena River Delta in the southern Laptev Sea has an approximate center point at 72°N and 126°E and is the largest of the arctic deltas. It covers about 32 000 km² and is highly dissected by rivers and streams with more than 1 500 islands [*Are and Reimnitz*, 2000]. The mean annual discharge between 1999 and 2008 of the Lena River into the Delta area and the Laptev Sea amounts to 588 km³ from a contributing watershed area of 2.46 10⁶ km² [*Holmes et al.*, 2012]. About 70 % of the riverine sediment discharge of the Laptev Sea is provided by the Lena River [*Rachold et al.*, 2000].

The Lena Delta is located in the zone of continuous permafrost with a maximum thickness of about 500 to 600 meter [*Romanovskii et al.*, 2004]. The basis for the present permafrost distribution in the region was the Middle to Late Pleistocene, when the global water level was about 120 m lower and the shoreline of the Arctic Ocean was several kilometers seawards of today's shore. The cold and dry climate led to permafrost aggradation in the study area on a flat accumulation plane in front of the Chekanovsky Ridge [*Schirrmeister et al.*, 2011] (Figure 3-1). The change of the environmental conditions to a warmer and wetter climate during the transition of the Late Pleistocene to the Holocene did promote permafrost degradation and thermokarst processes began to form the landscape [*Wetterich et al.*, 2008]. These have been active throughout the Holocene with varying intensity [*Romanovskii et al.*, 2004].

The Lena River Delta is situated in a neotectonic zone that is characterized by high seismic activity and resulting vertical movements of several blocks [*Are and Reimnitz*, 2000]. The extension of the Arctic Mid-Ocean Ridge into the Laptev Sea and uplift of the Siberian coast ridges are the main drivers for these processes [*Schwamborn et al.*, 2002]. These activities are important factors for today's complex structure of the delta channels and were most likely responsible for changing the major flow directions within the delta during the Holocene [*Schwamborn et al.*, 2002].
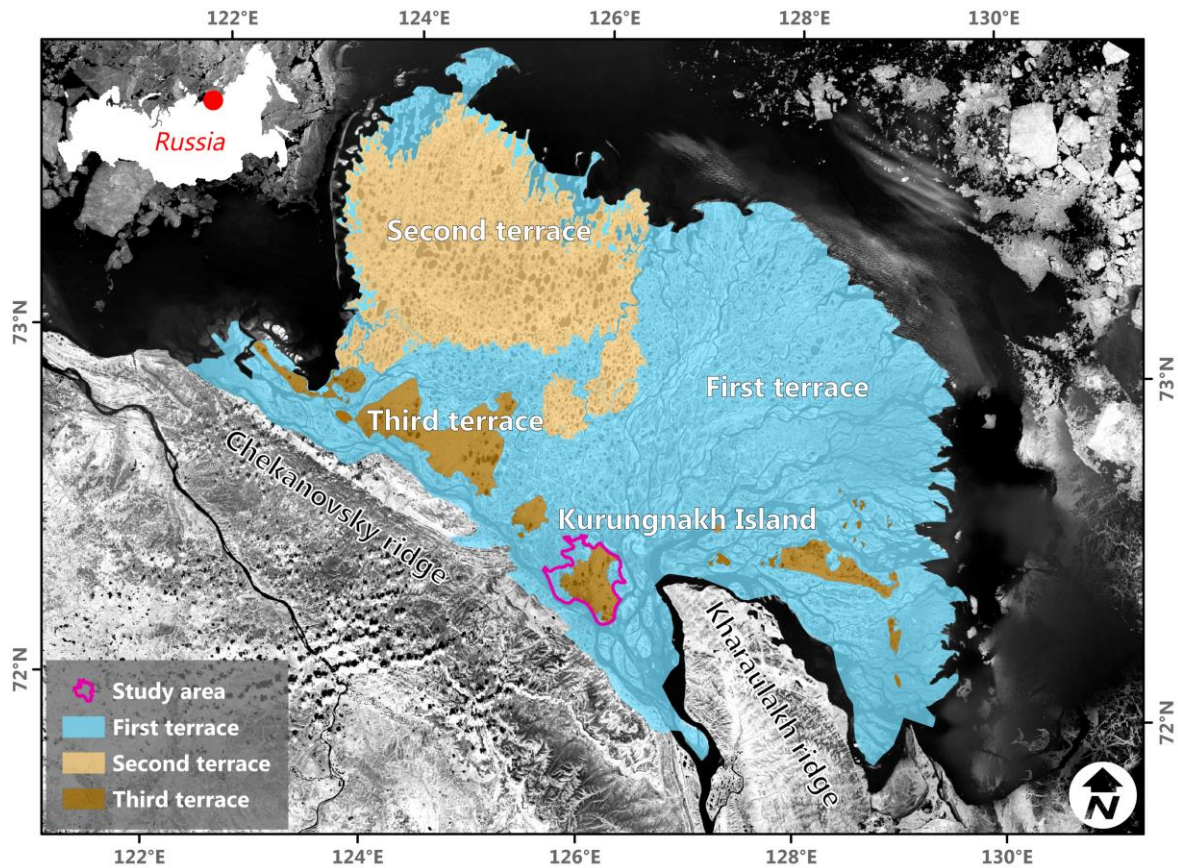
Figure 3-1: Geomorphological overview of the Lena River Delta and the location of the study area Kurungnakh Island. Background image from *MDA* [2004].

Three main geomorphologic units can be differentiated in the Lena Delta (Figure 3-1). The first main terrace is today's active delta with heights from 1-12 m above sea level (MASL) and has formed since the Middle Holocene. It covers mainly the eastern part of the delta and is characterized by patterned ground formed by ice-wedge polygons with relative ice-rich sediments or active floodplains without patterned ground and with low ice and organic contents. The second terrace with heights ranging from 11-30 MASL was formed during the Late Pleistocene to Early Holocene. Located in the northwestern part of the delta, it covers about 23 % of the delta area and is composed of sandy sediments with low ice contents. The polygonal micro relief is less expressed and more thermokarst activity is observed. The third main terrace ranges from 30-60 MASL and is the oldest part of the delta area. It's upper layer has not a fluvial-deltaic origin but today's islands in the south of the Delta represent erosional remnants of a Late Pleistocene accumulation plane consisting of fine grained, organic- and ice-rich sediments of the Chekanovsky Ridge and the Kharaulakh Ridge located in the south. Underneath these Ice Complex deposits are fluvial sands. The thickness of the active layer is usually in the range of 30–50 cm during summer.

The region is characterized by an arctic continental climate with strong variations over the year. While the mean annual air temperature is −13°C, the mean temperature in January

11

is −32°C and 6.5°C in July. The mean annual precipitation is low and amounts to about 190 mm (WWIS, 2004). Precipitation is occurring mostly in summer between the middle of May and the end of September with a mean of 125 mm between the years 1999 and 2011. 70% of these rainfall events are characterized as light rainfall events with 1 mm precipitation and only 1% of the measured events are characterized as heavy precipitation events (precipitation > 16mm) [*Boike et al.*, 2013].

Snow plays an important and complex role in the periglacial geomorphology by limiting the heat transfer between the atmosphere and the ground, thus mean ground temperatures are warmer than the mean air temperatures during winter [*Stieglitz et al.*, 2003]. The snow also forms patches in depressions and valleys that can last longer and lead to surface erosion from flowing water upon melting. Furthermore, eolian input remains on the snow patches and leads to the formation of debris near the snow patch [*Kunitsky et al.*, 2002]. In the Lena Delta a snow cover is developing in October that breaks up again in July. Its average thickness is about 40 cm, but strong variations can occur when the winter storms transport the snow, particularly in incised areas like valleys and thermokarst depressions. In these protected areas snow banks can remain during the summer (Figure 3-2).

Figure 3-2: „Lucky Lake Valley“ middle catchment in summer (left) and spring (right) with snow patch overlain by eolian sediments. Left image taken at 12th of July 2013, right image taken by Antje Eulenburg at 16th of June 2014.

Due to the harsh climate conditions and a distinct solar seasonality, plant growth is limited. Almost no photosynthetic activity is observed during the polar night from October until March, while in summer during polar day photosynthesis is possible all day. Consequently the Lena Delta is covered by typical tundra vegetation of various types. Major components are grasses, sedges, mosses, lichens, herbs, and dwarf shrubs [*Kutzbach et al.*, 2004].

The study area of Kurungnakh Island is made up of the first and third terraces and comprises polygonal ponds and thermokarst lakes, alasses, undisturbed Ice Complex surfaces and thermo-erosional valleys (Figure 3-3). As Morgenstern et al. [2014] states, similar sites

west of the Lena Delta feature more thermo-erosional permafrost degradation features, while comparable sites east of the Lena Delta are dominated by the presence of thermokarst. Thus, the geomorphological situation on Kurungnakh Island with a mixture of both processes and related landforms is special and offers the opportunity to study the interaction of both processes.
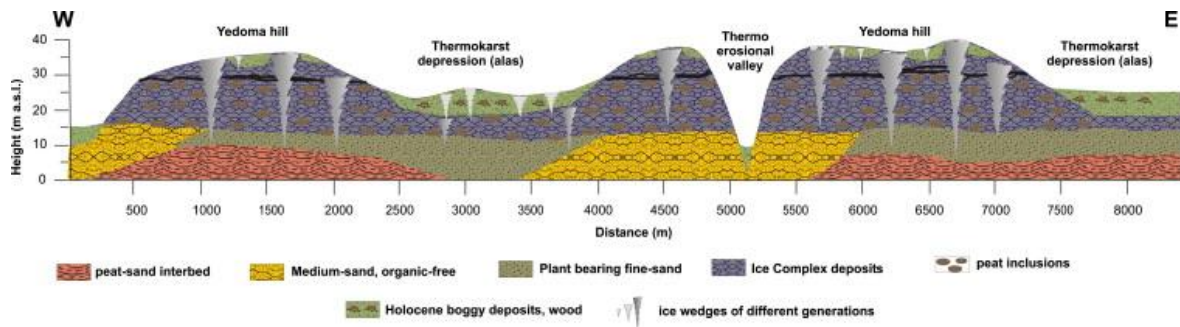
Figure 3-3: Generalized cross-section of exposures along the Olenyokskaya Channel at the eastern coast of Kurungnakh Island. From *Schirrmeister et al.* [2011].

Kurungnakh Island comprises some low lying areas covering the island's northeastern part, a small part in the south, the western border and the northern part of the island. These areas belong to the active floodplain system of the Lena River Delta channels. An extensive alas valley with north-south orientation is located in the central part of the island. Higher elevated regions located east and west of the alas valley represent the Ice Complex surface with maximum heights of 55 MASL [*Morgenstern et al.*, 2013]. Within the Ice Complex, several alas depressions are incised into the surface and are often connected with the surrounding delta channels through thermo-erosional valleys.

In this study three sites are of major importance, the "Drained Lake Valley" (DLV) at the eastern coast, the "Lucky Lake valley" (LLV) in the south and the "Main Valley" (MV) in the western part of the island (Figure 3-4). Each of them represents different stages of valley evolution, thus permafrost degradation, since they are positioned in a) Ice Complex, b) a transitional zone of the third and the first terrace and c) Ice Complex that is severely degraded by thermokarst.
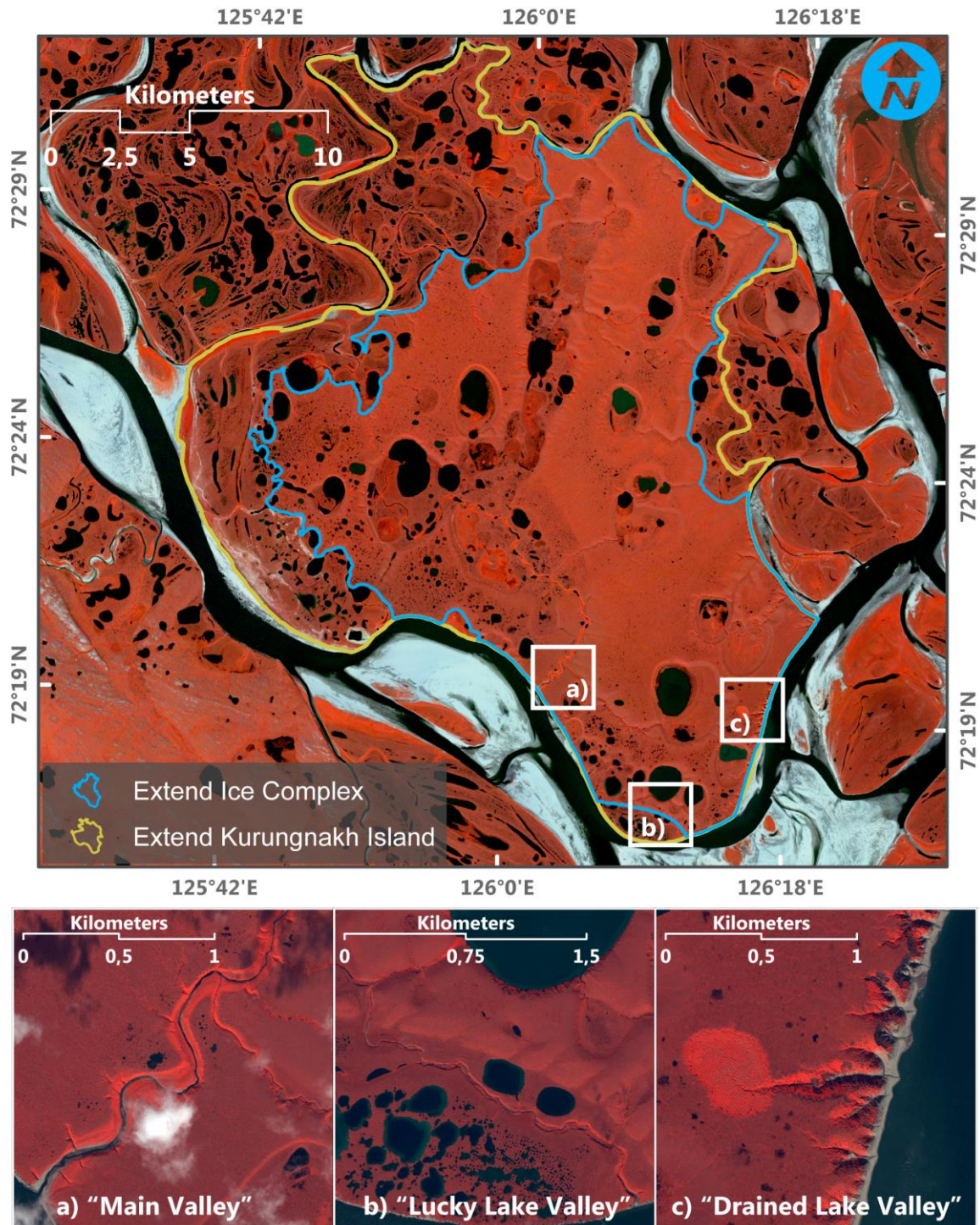
Figure 3-4: Kurungnakh Island and the three key sites a) "Main Valley", b) "Lucky Lake Valley" and c) "Drained Lake Valley". Background image top: RapidEye, band combination 5,2,1, projection UTM Zone 52N within WGS 84 datum. Background image of the key sites: GeoEye-1, band combination 4,2,1; projection UTM Zone 52N within WGS 84 datum.

4   Methods

The methodological approach of this work is to combine fieldwork, photogrammetric and remote sensing techniques and morphometric and spatial analysis in order to quantify and understand thermo-erosional processes that take place in ice-rich permafrost deposits of Kurungnakh Island. The following major tasks have been performed: 1) obtaining ground truth data in the field; 2) multisensory satellite image fusion; 3) generation of a high-resolution DEM for Kurungnakh Island; 4), mapping of thermo-erosional features and 5) morphometric and spatial analysis of thermo-erosional features. Figure 4-1 shows the general study scheme.
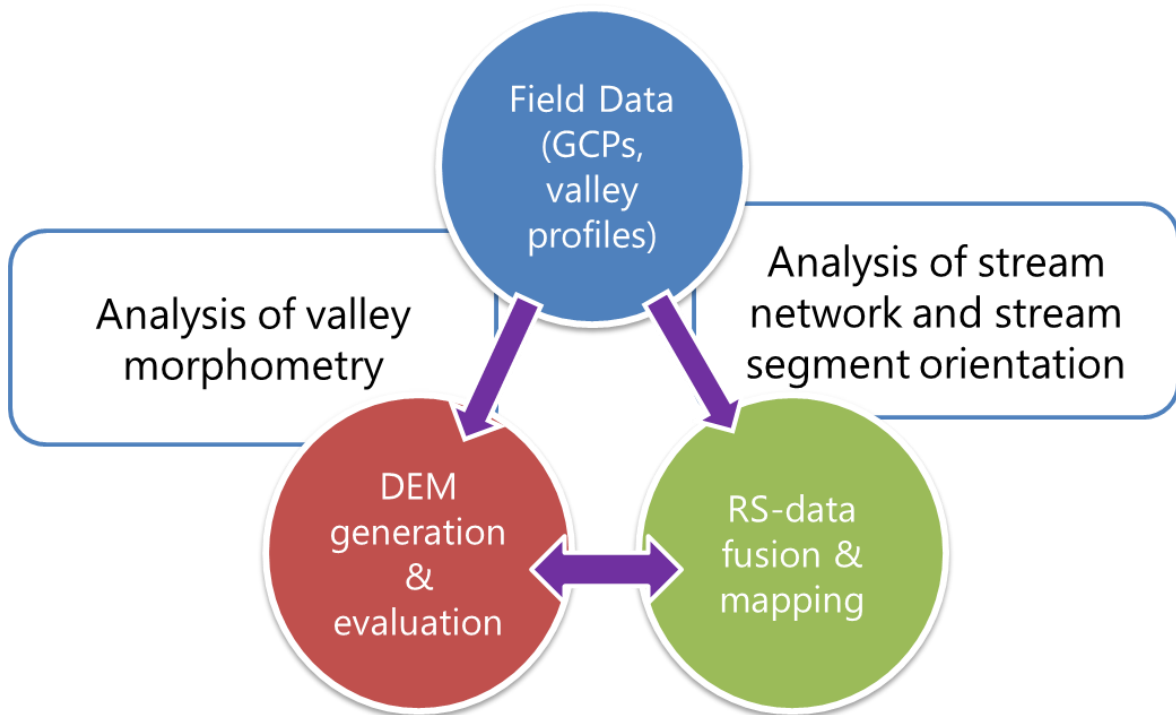
Figure 4-1: Overview of the methodological approach.

The geometric correction of satellite data and the DEM generation were performed using PCI Geomatica's software package Ortho Engine 2013. DEM evaluation, mapping as well as morphometric and spatial analyses were done using the geographical information system (GIS) ArcGIS 10.2 of ESRI.

4.1   Fieldwork

Field data were obtained during an expedition to the Lena River Delta in July 2013. Fieldwork included the description of general surface and relief properties of the landscape as well as precise geodetic surveys of ground control points (GCPs) and thermo-erosional landforms. These surveys were conducted using a Leica Viva global navigation satellite system (GNSS) system operating in real-time kinematic mode (RTK). Surveys with RTK GNSS are very

attractive for high-accuracy and high-productivity global positioning system (GPS) surveying, since they can deliver positioning accuracies of ± 2 cm in a few seconds [*Hasegawa et al.*, 2000; *Hauck*, 2013]. Within RTK mode two GPS receivers are set up (base and rover, see Figure 4-2) that take simultaneous measurements and are communicating over radio connection. When the base coordinates and measurements are processed to resolve the ambiguity and sent to the rover, it obtains centimeter-level positioning accuracy due to phase observation [*Lillesand et al.*, 2004; *Mekik and Arslanoglu*, 2009]. The projection was set to geographic WGS 84 co-ordinate system. Because radio signal loss occurred within a distance of about 2 km a base station was set up in every study site. The dataset was exported from the device as .html file, modified within a table and imported as .txt in the GIS. Coordinates were re-projected to UTM WGS 84 zone 52 N.
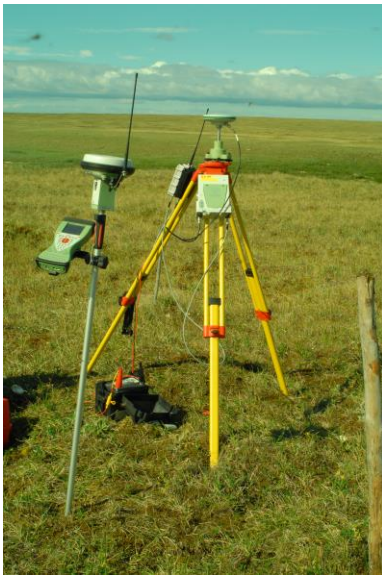
Figure 4-2: Set up of GPS in RTK mode. Left: RTK rover with GPS- and radio antenna, right: base station with GPS-antenna and radio connected to a 12V battery.

GCPs are identifiable non-moving features that are used for the geometric correction of remote sensing data. The collection of GCPs is difficult in tundra environments because they are highly dynamic due to freeze and thaw processes, and also the absence of anthropogenic features like road crossings. During the field campaign eleven GCPs were collected, mostly at the edges of small ponds, at interconnections of polygon rims and at outflows of small thermokarst lakes.

Thermo-erosional landforms were mainly surveyed in transversal and longitudinal profiles. Transversal profiles were measured at representative locations of different valley segments, beginning from and ending at the terrain surface, i.e. the uphill Ice Complex surface. However, the discrimination of the terrain surface is often challenging in tundra landscapes because of low height gradients and the resulting gentle slopes. A break line of the valley profiles is mostly not visible in the field. The profile points were measured at positions with a significant change in slope gradient.

Overall 44 profiles were taken in three key sites during the field campaign:

- "Main Valley":   11 transversal and 1 longitudinal.

- "Drained Lake Valley":   5 transversal and 2 longitudinal.

- "Lucky Lake Valley":   12 transversal and 1 longitudinal.

4.2   Image fusion

"Image fusion refers to the acquisition, processing and synergistic combination of information provided by various sensors or by the same sensor in many measuring contexts." *Simone et al.* [2002]. The Registration of multiple source imagery in this context is one of the most important issues when dealing with remote sensing data [*Moigne et al.*, 2011]

In order to provide a consistent image of thermo-erosional landforms for Kurungnakh Island a common best-practice strategy of image selection, fusion, examination and analysis was applied. Using multi-temporal and multi-platform remotely sensed data, various distortions associated with the platform, the map projection and the shape of the study area surface have to be considered. In this study high and very high spatial resolution optical space-borne imagery with differing geometric characteristics were used (see Table 4-1). All images were acquired at different times and oblique viewing and azimuth angles.

Conventional 2-D polynomial rectification functions do not correct for relief induced and image acquisition system distortions, and 2-D ground control points only correct for local distortions and are very sensitive to input errors [*Toutin*, 2004]. Therefore block adjustment and subsequent orthorectification using rational polynomial coefficients (RPC) in PCI Geomatica's 2013 module Ortho Engine was performed. RPC models are derived from the physical sensor model to describe the object-image geometry and to transform three-dimensional object-space coordinates into two-dimensional image-space coordinates [*Grodecki and Dial*, 2003]. *Fraser and Ravanbakhsh* [2009] report geopositioning accuracies for GeoEye-1 images of 0.1 m in planimetry and 0.25 m in height using a single GCP within an RPC model.

Table 4-1: Overview of used remote sensing data, their characteristics and results of the geometric correction.

Sensor	No. of scenes	Date yyyy/mm/dd	Ground resolution [m]	RMSE [m]	Number of GCPs
GeoEye-1	2	2010/05/08	0.5 / 2.0	0.36	4
RapidEye	1	2010/07/05	6.5	2.86	17
ALOS PRISM	6 4	2006/09/21 2009/09/12	2.5	2.34	195

The basis for the registration of the GeoEye-1 and RapidEye scenes is the network of high accuracy GCPs from the RTK survey. For the registration of the GeoEye-1 scenes, that were pansharpened using the algorithm developed by *Yun* [2002], very good results with sub meter accuracy were obtained using 4 GCPs (Table 4-1). Because the GeoEye-1 scenes only cover the southern part of Kurungnakh Island, a RapidEye scene was registered with combined GCPs and planimetric information from GeoEye-1 and height information from topographic maps; RapidEye imagery also has RPC information and combines high spatial resolution with considerable coverage. The scenes from the "Panchromatic Remote-sensing Instrument for Stereo Mapping" (PRISM) on board of the "Advanced Land Observation Satellite" (ALOS) were finally registered on the basis of the Rapid Eye scene with the satellite orbital model by *Toutin* [2004] implemented in Ortho Engine. Neighboring and overlapping scenes were handled as joint photogrammetric image blocks to get higher redundancy in the image model.

4.3 DEM generation

Overlapping satellite images (stereopairs) provide the opportunity to extract height information for subsequent DEM generation using the principle of image parallax. The term parallax refers to the apparent change in relative positions of stationary objects caused by a change in viewing position [*Lillesand et al.*, 2004].

ALOS PRISM carries a three line scanner instrument, which provides high-resolution panchromatic optical images. These images of about 2.5 m ground sampling distance are acquired in the same orbit in nadir and respectively 23.8° forward and backward directions, providing a base to height ratio (B/H) of 1 (see Figure 4-3) [*JAXA*, 2008]. The base to height ratio is the distance on the ground between two centers of overlapping images, divided by the aircraft altitude. Values between 0.5 and 1 are reported to be reasonable for DEM extraction [*Hasegawa et al.*, 2000].
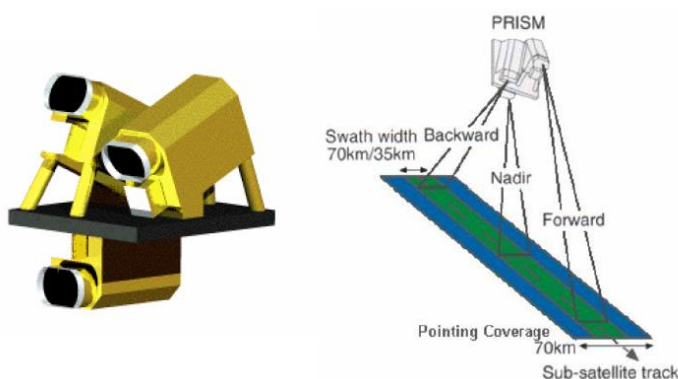
Figure 4-3: Configuration of the PRISM sensor on board of the ALOS platform. *Takaku et al.* [2007]

Based on these overlapping images high-resolution DEMs resembling the visible surface in ground sampling distances of about 2.5 to 10 m can be derived.; These are comparable to height information from topographic maps with the scale of 1:25 000 [*Takaku et al.*, 2007]. However, for images of the ALOS PRISM sensor with acquisition dates before early 2007, radiometric quality problems due to black reference calibration, jpeg-compression and saturation effects are reported that result in effects of striping and blocking [*Gruen and Wolff*, 2007]. These effects combined with the homogenous Tundra landscape can severely affect the matching process during DEM extraction. The algorithm by *Kamiya* [2008] was applied to reduce the jpeg-noise effects for the images with acquisition date of 2006.

4.3.1   DEM scenarios

Six images from 2006 and four from 2009 totaling 14 combinations of stereopairs were used for DEM generation (see Table 4-2 and Table 4-3). It is common in classical photogrammetry to use only a generic triplet, consisting of a backward, a nadir and a forward looking-image. In this study additional images were included in the DEM generation process to address the following problems: 1) A consolidation of the data could improve the results of the image matching process on homogenous Ice Complex uplands with low contrast and low slope gradient that are expected to be insufficient; 2) Adding images with different viewing angles to the DEM extraction process could decrease the effect of occlusion that occurs especially at the bottom of steep valleys; 3) Adding Images of 2009 will decrease errors in the orthorectification process of GeoEye-1 and RapidEye images, because effects of coastal erosion on the eastern coast of the study area are considered in a combined DEM. 10 DEM scenarios with differing combinations of stereopairs were tested during the DEM generation process (Table 4-4).

Table 4-2: Overview of the ALOS PRISM dataset

Acquisition date	Scene ID	Mode	Internal ID
21.09.2006	ALPSMB035022170-O1B1__B	Backward	2006-2170-B
	ALPSMN035022115-O1B1__N	Nadir	2006-2115-N
	ALPSMF035022060-O1B1__F	Forward	2006-2060-F
	ALPSMB035022175-O1B1__B	Backward	2006-2175-B
	ALPSMN035022120-O1B1__N	Nadir	2006-2120-N
	ALPSMF035022055-O1B1__F	Forward	2006-2055-F
12.09.2009	ALPSMB193582170-O1B1__B	Backward	2009-2170-B
	ALPSMW193582115-O1B1__W	Wide	2009-2115-W
	ALPSMB193582175-O1B1__B	Backward	2009-2175-B
	ALPSMW193582120-O1B1__W	Wide	2009-2120-W

Table 4-3: Possible combinations of stereopairs for DEM extraction. Names correspond to the Internal ID field in table 4-2. Stereopairs with ID 1-12 are expected to have B/H ratios within the range 0f 0.5 to 1, while Stereopairs 13 and 14 are to be expected to exceed a B/H ratio of 1.

Stereopair ID	Left	Right
1	2006-2170-B	2006-2115-N
2	2006-2170-B	2006-2060-F
3	2006-2115-N	2006-2060-F
4	2006-2175-B	2006-2120-N
5	2009-2170-B	2009-2115-W
6	2009-2175-B	2009-2120-W
7	2006-2170-B	2006-2120-N
8	2006-2115-N	2006-2175-B
9	2006-2115-N	2006-2055-F
10	2006-2060-F	2006-2120-N
11	2009-2170-B	2009-2120-W
12	2009-2175-B	2009-2115-W
13	2006-2170-B	2006-2055-F
14	2006-2175-B	2006-2060-F

Table 4-4: Overview of DEM generation scenarios that were processed and evaluated. Numbers in the second column correspond to the Stereopair ID in Table 4-3.

Scenario ID	Stereopairs
Triplet	1 / 2 / 3
Green06	1 / 2 / 3 / 4
Green09	5 / 6
Green0609	1 / 2 / 3 / 4 / 5 / 6
Greenorange06	1 / 2 / 3 / 4 / 7 / 8 / 9 / 10
Greenorange09	5 / 6 / 11 / 12
Greenorange0609	1 / 2 / 3 / 4 / 5 / 6 / 7 / 8 / 9 / 10 / 11 / 12
Greenred06	1 / 2 / 3 / 4 / 13 / 14
Allc06	1 / 2 / 3 / 4 / 5 / 7 / 8 / 9 / 10 / 13 / 14
Allc0609	1 / 2 / 3 / 4 / 5 / 6 / 7 / 8 / 9 / 10 / 11 / 12 / 13 / 14

4.3.2 DEM extraction

The process of generating a DEM consists of several steps: 1) converting the raw images into epipolar pairs; 2) extract DEMs from the overlap between the epipolar pairs; 3) geocode the epipolar DEMs on the basis of the geometric model and stitch them together to form one DEM and 4) edit poorly correlated areas in the DEM.

During epipolar resampling stereo pairs are reprojected, so that they have a common orientation and the matching features appear on a common x-axis (Figure 4-4). This reduces computation time because a smaller search window is needed and the possibility of incorrect matches is reduced.
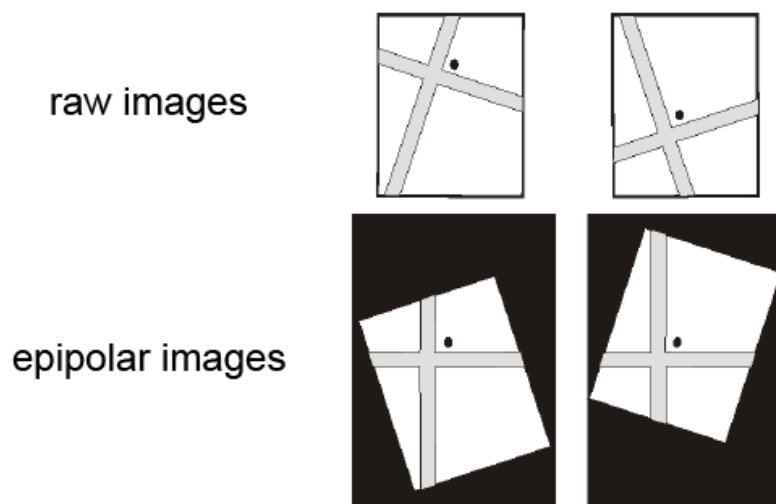
In the process of DEM extraction the parallaxes that correspond to terrain heights are calculated for every selected stereopair and are stored in a raster file that is finally geocoded. Within the ortho engine software package the extraction parameters were set as described in table 4-5.

Table 4-5: Selected parameters for the DEM extraction process within the ortho engine software package.

Parameter	Settings	Remarks
Minimum elevation	-49	Negative values are included in the DEM extraction process first.
Maximum elevation	80	Height values for the third terrace are reported not to exceed 80 MASL
DEM detail	Extra high	Image matching (correlation) is performed on images at full resolution to achieve precise representation of the terrain in the DEM.
Terrain type	Flat	This parameter is influencing the size of the image matching window. Since the study area is located in polar lowlands the terrain type can be regarded flat.
Fill holes (smoothing filter)	Low	Not correlated areas will be interpolated. In this study smoothing was set to a minimum to preserve actual elevation values.
Create score channel	Yes	The score channel gives information about the correlation of corresponding features in the stereopairs. It is a quality parameter of the image matching process and is stored in an additional image channel.
Create geocoded DEM	Yes	Based on the GCPs in the geometric correction model the final DEM is geocoded to UTM Zone 52N in the WGS 84 datum.
Resolution	20x20 / 5x5	To compare different DEM scenarios with different parameters and to reduce computation time the resolution was set to 20x20 meter. The final DEMs were resampled to 5x5 meter.
Output option	Average	The output DEM is containing the average value of all stereopair DEMs in one scenario.

4.3.3   DEM editing

The produced DEMs contain pixels with failed and incorrect values (artifacts). Therefore, the DEM from the scenario Triplet was edited to smooth out irregularities and create a more pleasing DEM that is suitable for presentational use and for orthorectification of the satellite images. The raw DEM from the scenario Green0609 was not edited because it showed the best results in the evaluation process and edited products had decreasing quality parameter values.

Water bodies are a major source for artifacts. Here the image matching produces values that are far out of the general failure range. This is due to the very low contrast of water bodies and their constantly changing values in between the different images acquisitions. Therefore it is necessary to modify the areas of the DEM that represent lakes and the Lena River channels. Another observed artifact in the DEMs is a wavy like noise structure throughout the whole scene. This problem is addressed by smoothing approaches.

The water bodies of Kurungnakh Island were automatically extracted using a grey-value thresholding on RapidEye's infrared channel, which absorbs the light very strong in the infrared wavelength of the electromagnetic spectrum. A threshold value of 1 000 of the Digital Number (DN) of the band was used and the results were visually evaluated. The DN value in RapidEye datasets is radiometrically corrected on-ground and the original sensor bit depth of 12 bit is scaled to 16 bit dynamic range. Therefore, the resulting DN values are directly related to the absolute at sensor radiances [*Blackbridge*, 2013]. The produced raster dataset was converted to a vector shapefile and only water bodies with a size greater than 25 000 square meters were used. The shapefile was then clipped to the extent of Kurungnakh Island. The DEM values under the resulting water mask were first set to "NoData" and then interpolated from the surrounding lake coasts. These areas show very good matching results, because the water-land transition zones have a high contrast along the shore. Following the interpolation the values under the mask were smoothed using a 3x3 window. Finally, the average value of each lake shape is calculated and assigned to the pixels beneath.

The Lena River Delta channels were extracted using the same grey-value thresholding method described above. The produced shapefile was additionally adjusted using beach-water transition lines digitized form an ALOS PRISM scene to get the same extent as the DEM. Values under the Lena Delta River channel mask were assigned to values of 1 that represent the expected water level of the Delta.

Noise related artifacts were partly removed using two 9x9 sized filters implemented in the ortho engine environment. The first filter excludes failed and background pixels based on calculated averages and variances of the eight elevation values immediately surrounding each

pixel; if the center pixel is more than two standard deviations away from the average it is replaced with the failed value. The second filter counts the number of failed values immediately surrounding each pixel. If five or more failed pixels border the center pixel, then the center pixel is also set to a failed value [*PCI-Geomatics*, 2013]. The identified failed pixels are then interpolated using an estimate weighted by distance calculated from the valid surrounding pixels. The DEM is then twice smoothed using a 3x3 sized Gaussian filter window that calculates the weighted sum within the window and assigns the value to the center pixel.

4.4 DEM evaluation

The quality of the produced DEMs was evaluated with a multilevel approach using the score channel that is produced during DEM extraction and 1 024 points from the RTK-GPS survey. For every extracted DEM a score channel was exported that gives information about the quality of the image matching process. In this raster channel values of 0 and 50-100 are stored that represent the correlation of two images. The score channel was clipped to the extent of Kurungnakh Island and the percentage of zero values, i.e. not correlated area were no heights could be extracted and the means of the remaining values were stored in a table.

Elevations of the DEM were extracted at the position of the GPS points and subtracted from the GPS values. The resulting deviations were then classified according to their absolute relief height in two-meter steps from 0 to 58 MASL, resulting in 28 classes. This way, deviations of the DEMs can be visualized according to their absolute height. For every elevation class the median value of the deviations was calculated. The standard deviation of all medians for every elevation class was used as an internal quality parameter to compare the different DEM scenarios. A linear trend was calculated from the deviations and applied to the raw DEM on a pixel by pixel basis. The resulting trend surface was then subtracted from the raw DEM to achieve the corrected DEM.

The overall relative root mean square error (RMSE$_r$) of the vertical deviations was calculated using the following formula:

$$RMSE_r = \sqrt{\frac{1}{n}(\delta h_1{}^2 + \delta h_2{}^2 + \cdots + (\delta h_n^2)},$$

where

n   =   number of evaluation points,

δh =   Elevation difference of GPS and DEM

It represents the height deviations at the location of the GPS points. This value was then combined with the overall RMS of the DGPS points (RMSE_d) using the following formula,

$$RMSE_a = \sqrt{(RMSE_r^2 + RMSE_d{}^2)}$$

to obtain the absolute vertical accuracy of the DEMs. The planimetric accuracy of the DEM is defined by the result of the geometric correction model shown in table 4-1, chapter 4.2.

4.5   Mapping

Thermo-erosional valleys, the upper margins of thermokarst basins, the Ice Complex extent and the shoreline of Kurungnakh Island were mapped on the basis of GeoEye-1, RapidEye and ALOS PRISM images in a GIS using a scale of 1:3 000. The main characteristics of the datasets are listed in table 4-6.

Only thermo erosional features that are visible in the ALOS PRISM datasets were digitized to preserve a consistent dataset. The RapidEye scene was used with the near infrared and red edge channel displayed on the red channel. This combination of bands especially helps to identify wet areas and therefore makes the incised valleys with concentrated water from the surroundings visible when the path of the stream is not clearly visible in the ALOS PRISM dataset.

Table 4-6: Overview of the datasets derived from the mapping process. A vertex (plural vertices) is a point that describes the corners of intersections of geometric shapes.

Dataset	Data Type	Number of features	comment	purpose
Streams	Polyline	855	On the basis of GeoEye-1, RapidEye and ALOS PRISM	Stream network
Stream links	Polyline	1 214	Streams split at the intersections of each stream feature	Stream order and stream link orientation
Stream points	Point	17 823	Vertices of the digitizing process converted to point file	Extraction of height information for longitudinal profile plots
Basins	Polygon	22	Modified after *Morgenstern et al.* [2011], on the basis of RapidEye	Identify streams affected by thermo-karst
Shoreline Kurungnakh	Polygon	1	On the basis of ALOS PRISM and RapidEye	Clipping extent for DEM datasets
Ice Complex extent Kurungnakh	Polygon	1	Modified after *Morgenstern et al.* [2011], on the basis of GeoEye-1, RapidEye and ALOS PRISM	Clipping extent for stream dataset

The thermo-erosional features were digitized, beginning with the highest point and ending at the shoreline of Kurungnakh Island. Because the focus is on thermo-erosional valleys in the Ice Complex, the dataset was clipped to the extent of the Ice Complex. The dataset was clipped at the interconnections of each stream. The vertices of each stream dataset were converted to a point dataset and elevations from the DEM were extracted to get a dataset of longitudinal profiles.

The upper margins of the thermokarst basins were mapped on the basis of an existing shapefile produced by *Morgenstern et al.* [2011] and the RapidEye Scene. Because of a differing reference basis it was necessary to remap the features.

Shoreline mapping of Kurungnakh Island was done using a nadir viewing ALOS PRISM scene of 2006. It covers the entire island and all parts of the DEMs are included. The dataset was checked against the RapidEye scene to diminish effects of different water levels.

4.6 Morphometric analyses

According to *Evans and Minar* [2011] morphometric variables are to be divided into field variables and object variables. When looking at the stream networks of the mapped thermo-erosional features, object variables of linear nature are extracted, such as stream order, stream length, stream direction and drainage density. Analyses regarding the direct morphology of the valley profiles in this case are field variables specific to the gravity field, such as altitude, slope gradient, slope aspect and curvature.

The stream order of a landscape is a dimensionless parameter that is referring to the interrelated drainage pattern that is formed by a set of streams in a certain area, from any number of sources down to the mouth, or root point, of the net [*Ranalli and Scheidegger*, 1968]. In the Strahler method of stream ordering, first order streams represent anterior tributaries of a stream network. These streams then merge to form second order streams, which also converge to form third order streams and so on for larger orders [*Strahler*, 1957]. The Strahler method does take into account stream links, and the order of a stream can change along the same stream (Figure 4-5). All fingertip tributaries of a stream network are assigned a value of 1. It is a suitable method of stream ordering to detect the organizational complexity of a stream network.
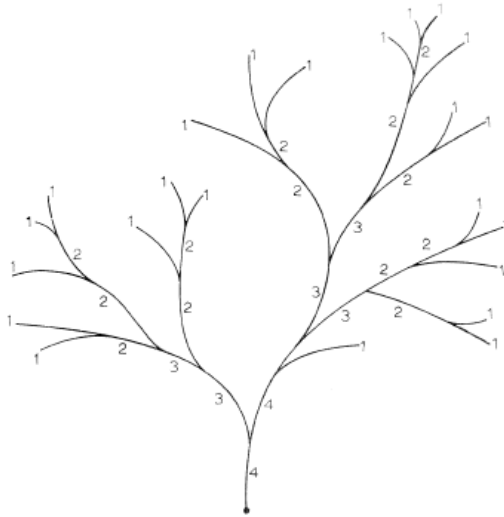
Figure 4-5: Strahler stream orders. In: Ranalli and Scheidegger [1968].

The stream order of the identified features was assigned manually to the stream link dataset and stored in a feature class table. For every stream link the mean direction and mean length was extracted using the "Linear Directional Mean" tool of the spatial statistics toolbox in ArcGIS 10.2. The resulting values range from 1 to 360 representing the Compass Angle in° beginning clockwise from due north.

The morphometric analyses of the transversal and longitudinal profiles are based on the field measurements and the raw DEM of scenario Green0609. Mean slopes were calculated for the right and left side of the transversal profiles where the point with the lowest elevation defines the center point of the profile and the first and the last point of the profile define the endpoints of the lines. Slopes were calculated from the RTK-GPS elevations and from the DEM elevations. Slopes were calculated between every RTK-GPS point of every profile and compared to the DEM values (Figure 4-6). Based on the stream dataset a shapefile containing all longitudinal profiles of Kurungnakh Island was created and the parameters, highest point, lowest point, height difference, length and slope were calculated.
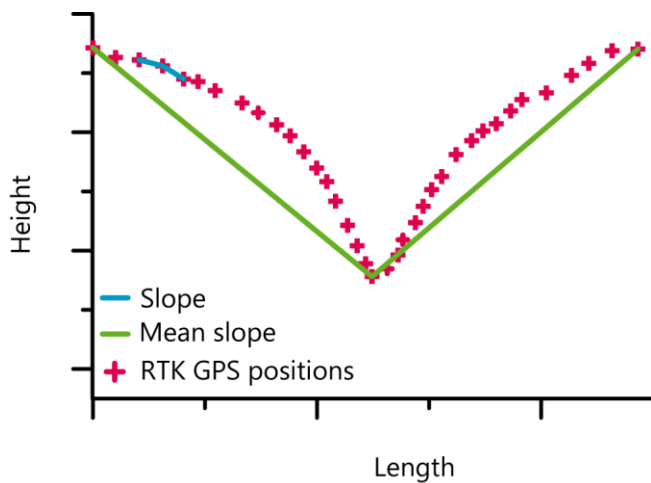
Figure 4-6: Scheme of a transversal profile and the extracted parameters slope and mean slope.

.

26

5 Results

5.1 High-resolution DEMs

The results of the ten DEM generation scenarios are shown in figure 5-1. The DEMs have differing extents that are defined by the boundaries of the input images. DEMs that combine images from 2006 and 2009 show a sharp step in height from northeast to southwest direction in the western part of Kurungnakh Island. All DEMs show underestimated areas below zero MASL, especially in the northern part of the image extents and on the Lena River Delta channels. The highest elevations are in the southwestern area where the Chekanovsky Ridge is located. Since the maximum height that is to be expected during DEM extraction was assigned to 80 MASL, the values for the Chekanovsky Ridge are not representing actual height.

Table 5-1 shows the evaluation results of the DEM scenarios. Values of the mean score channel are ranging from minimum 70.87 for the Allc09 scenario to 77.42 in the Triplet scenario. The highest amount of non-correlated pixels (71.02 %) is observed in the scenario Green09 while the lowest amount of non-correlated pixels is found in scenario Greenorange0609 (42.83%). The quality parameter ranges from 2.11 in scenario Green0609 to 3.35 in scenario Green09. The scenario Green0609 has the lowest relative and absolute vertical RMSE with 4.05 m and 4.41 m respectively, while scenario Green09 shows relative and absolute RMSE of 5.76 and 6.01 m respectively. The scenarios that use the 2009 images (scenario Green09 and scenario Allc09) have the lowest values in the score channel and show the most uncorrelated pixels. However, scenario Allc09 has the fifth lowest absolute RMSE of 5.16 m. Scenarios Green0609, Triplet and Greenorange0609 show the highest number of correlated pixels and the lowest relative and absolute RMSE.

Figure 5-2 shows the deviations of the ten DEM scenarios to the GPS points against the relief height. The different DEMs present a variety of deviations, but all DEMs show a step of elevation deviations at about 13 MASL. Scenario Green09 has the greatest deviations and is generally overestimating actual relief height up to 12 m. Scenario Triplet and Green0609 are showing similar and the lowest variations. They underestimate terrain heights below 10 MASL, and above 10 MASL they slightly overestimate terrain heights. At terrain heights of about 35 MASL and towards 60 MASL median deviations exceed 4 m.
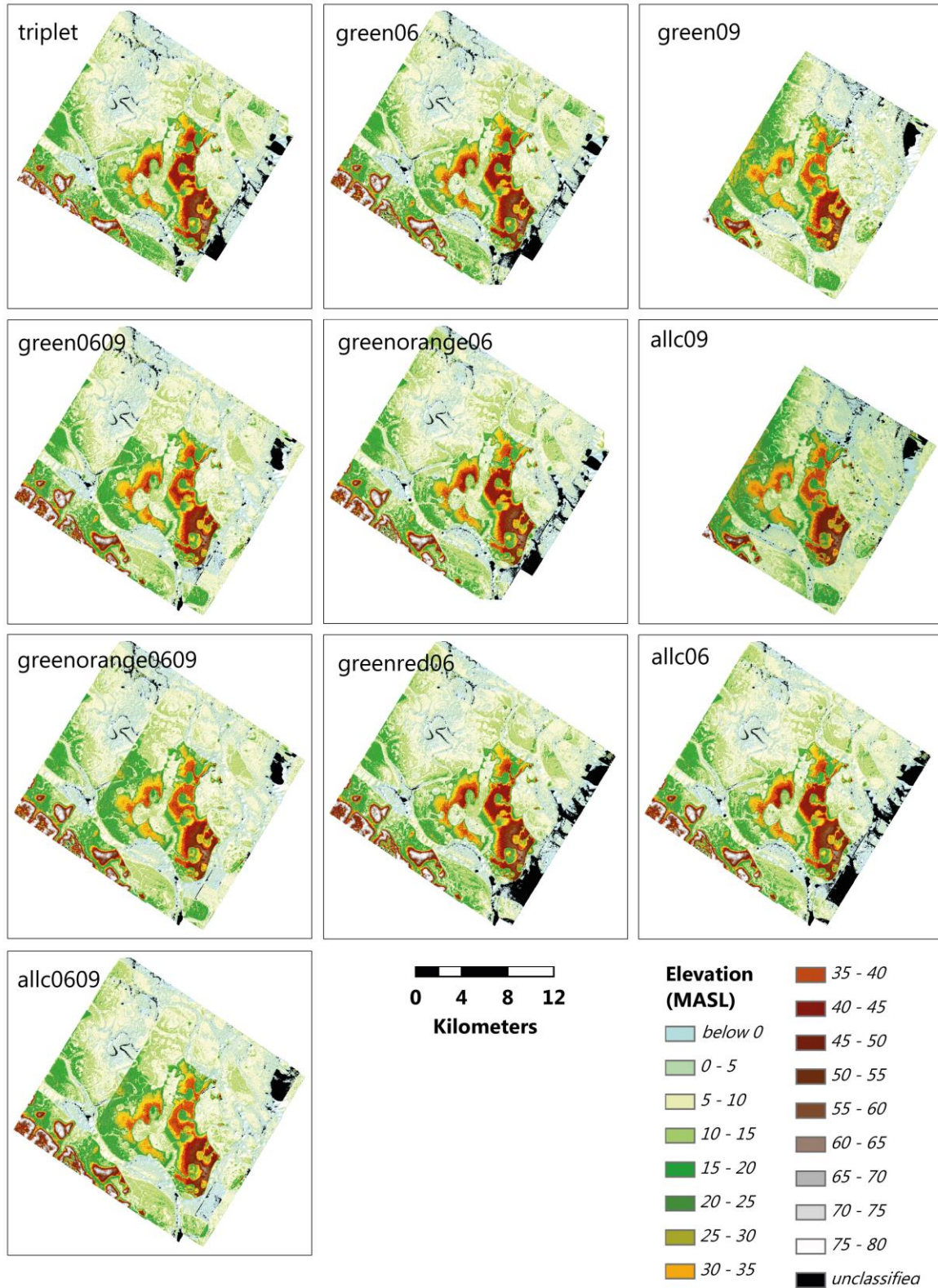
Figure 5-1: Results of the DEM generation scenarios. All DEMs are based on the same input parameters described in Table 4-5 and are resampled to 20x20 m ground resolution. Differences in the extent result from the differing input images with varying extents.
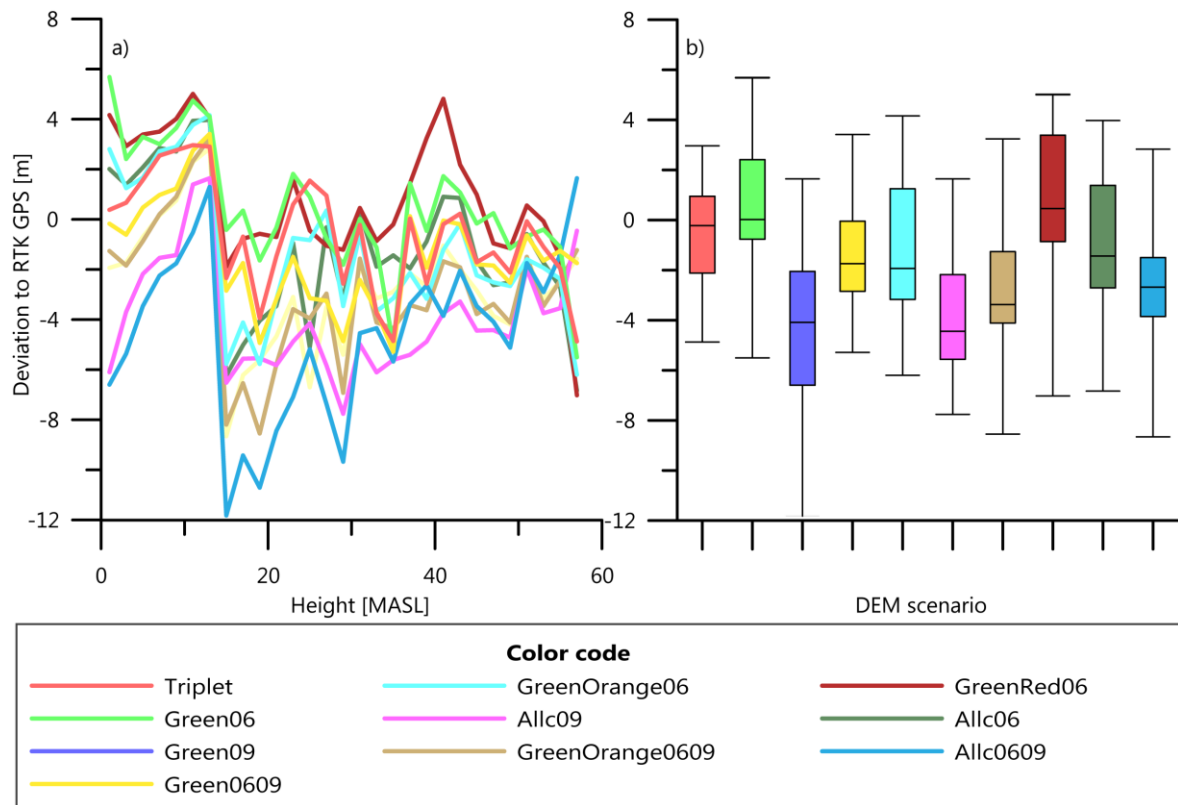
Figure 5-2: DEM error estimations and relief height: a) deviations of DEM scenarios with 20x20 meter ground sampling distance related to the terrain height. Positive and negative deviations occur when the DEM is underestimating and overestimating actual terrain height, respectively; b) every box-whisker plot represents one generated DEM. The color code in the legend corresponds to diagrams a) and b).

Two final DEMs were generated with 5x5 m spatial resolution: 1) the raw DEM of scenario Green0609 that showed the best results in the evaluation process and 2) the edited DEM from scenario Triplet which is not affected by the height step artifact and therefore is more suitable for presentational use and the orthorectification of satellite images.

Table 5-1: Evaluation results of the DEM generation process. The listed parameters are described in chapter 4.4.

DEM scenario	Mean score	Non-correlated pixels [%]	Quality parameter	Relative RMSE [m]	Absolute RMSE [m]
Green0609	77.40	42.99	2.11	4.05	4.41
Triplet	77.42	43.70	2.26	4.60	4.92
Greenorange0609	77.40	42.83	2.76	4.69	5.00
Allc0609	76.26	48.30	2.51	4.76	5.06
Allc09	70.87	67.41	2.26	4.86	5.16
Allc06	76.27	48.34	2.91	4.93	5.22
Greenorange06	76.46	47.44	2.84	4.93	5.22
Green06	77.42	43.16	2.55	5.08	5.36
Greenred06	76.64	47.30	2.63	5.16	5.44
Green09	71.06	71.02	3.35	5.76	6.01

Figure 5-3 shows the DEM from scenario Green0609, which is clipped to the extent of Kurungnakh Island. Its highest and lowest points are 79.3 MASL and 1.0 MASL respectively. The presented heights are decreasing from southeast towards northwest. In the central part of the island the wide alas valley cuts into the Ice Complex surface and has heights of 6 to 15 MASL of elevation. It represents the lowest parts of Kurungnakh Island that do not belong to the first terrace of the Lena River Delta. The directly surrounding Ice Complex surface has heights up to 45 MASL that increase towards southeast to up to 70 MASL. Thermokarst lakes are deeply incised into the Ice Complex surface and connected to the Lena Delta River channels through thermo-erosional valleys. The highest steps in elevation can be seen mostly on the east facing slopes of thermokarst lakes or the cliffs to the Lena River Delta channel while slightly more gentle slopes are on the west facing slopes. Some alas depressions feature frost heave hill structures in their center that are referred to as "Pingos" in periglacial geomorphology.

Some artifacts are visible in the DEM. The most prominent artifact is the already mentioned height step in the northwest of the scene that occurs in the DEMs with combined 2006 and 2009 images. This effect can occur when the GCP network in the corners of an image is not consistent. As a result the geometric correction model calculates wrong image geometry. Since this artifact occurs outside of the Ice Complex extent it is not of relevance for the analysis in this study. Some flat areas in the wide alas valley and on the first terrace of Kurungnakh Island between 1 and 15 MASL show some small scale noise in a patchy structure that is expressed in the DEM as small peaks and holes. Finally, some clouds in the 2006 input images lead to incorrect values in small parts in the northeast of the DEM.

Figure 5-5 shows the edited DEM from scenario Triplet. Compared to the DEM from scenario Green0609 (

figure 5-3), it shows a smoothed surface and does not have the sharp height step in the northwestern part of the island. Water bodies on lakes have a constant elevation and no areas with elevations below 0 MASL are present. Alas areas show more even and higher elevations than the DEM from scenario Green0609, especially in the central alas valley.
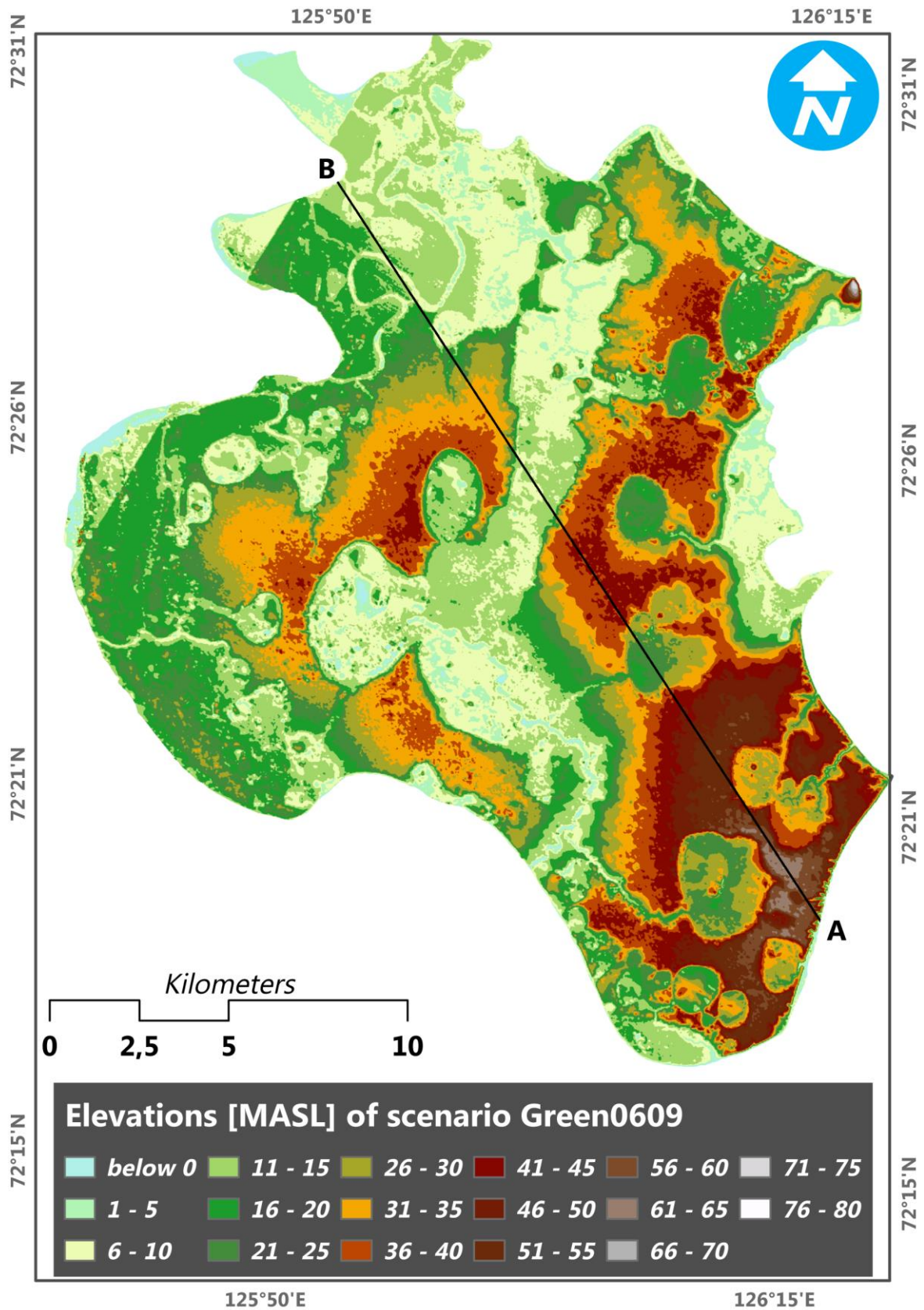
Figure 5-3: Classified DEM from scenario Green0609 with 5x5 m ground resolution. A and B show the start and end point of the topographic profile shown in figure 5-4.

Of interest are also the areas that are not correlated during image matching and that are interpolated during DEM generation (Figure 5-6). These areas are especially on the undisturbed low-contrast Ice Complex surface or the gentle alas slopes and water bodies where only few distinct features occur that can be detected during image matching. Sharp high contrast boundaries like shorelines of lakes or the Lena River Delta channels as well as thermo-erosional valleys and snow covered patches show high correlation values. The wide alas valley in the center and the northern parts of Kurungnakh Island are areas with high correlation values. Adding more images to the DEM extraction process did not significantly improve the correlation values or the percentage of non-correlated pixels (Table 5-1).

Kurungnakh Island has a decreasing height gradient that ranges from southeast to northwest with highest elevations around 70 MASL in the southeast near to the "Drained Lake Valley" site (Figure 5-4). The highly degraded alas valley in the central part of the island is in most parts only 11 MASL. The location with the highest elevations around 74 MASL is at the northeastern tip of the island and called "America Khaya".
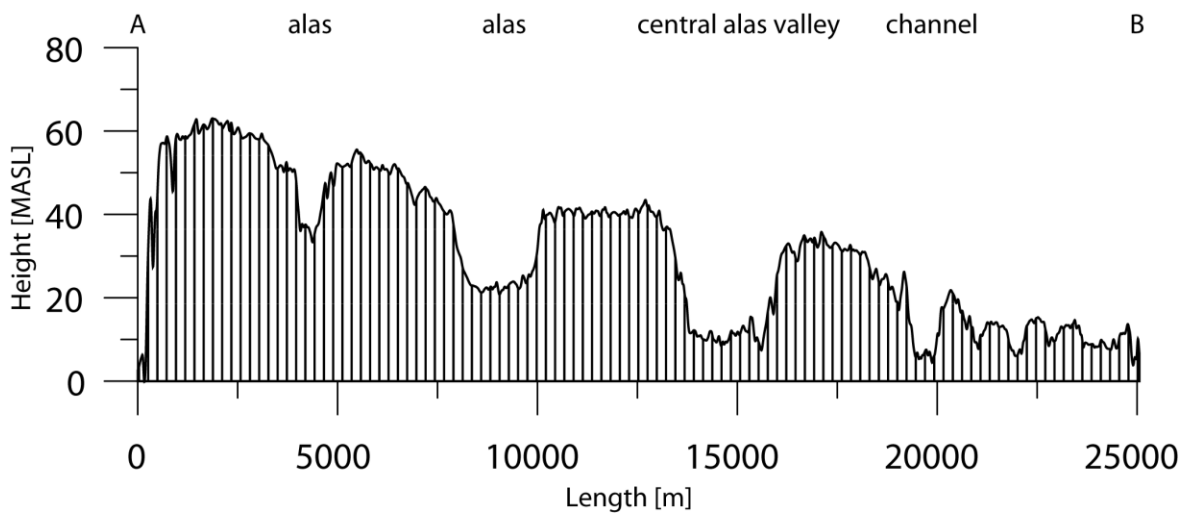
Figure 5-4: SE-NW topographic profile of Kurungnakh Island based on the DEM scenario Green0609. The location of the profile line is shown in (Figure 5-3)
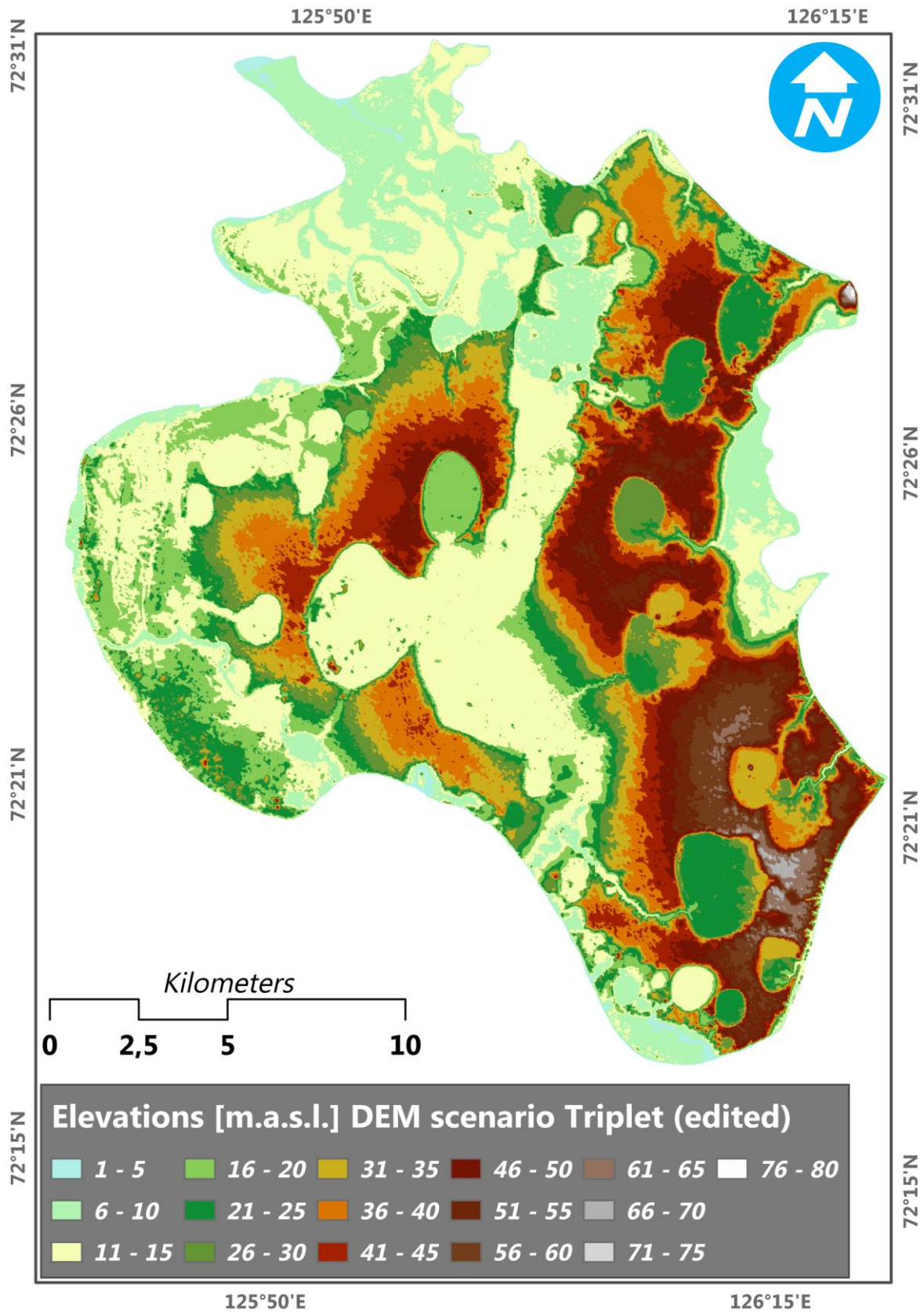
Figure 5-5: Classified DEM from scenario Triplet with 5x5 m ground resolution. Values below 1 m were assigned to a value of 1 m. The DEM was edited using the workflow described in chapter 0.
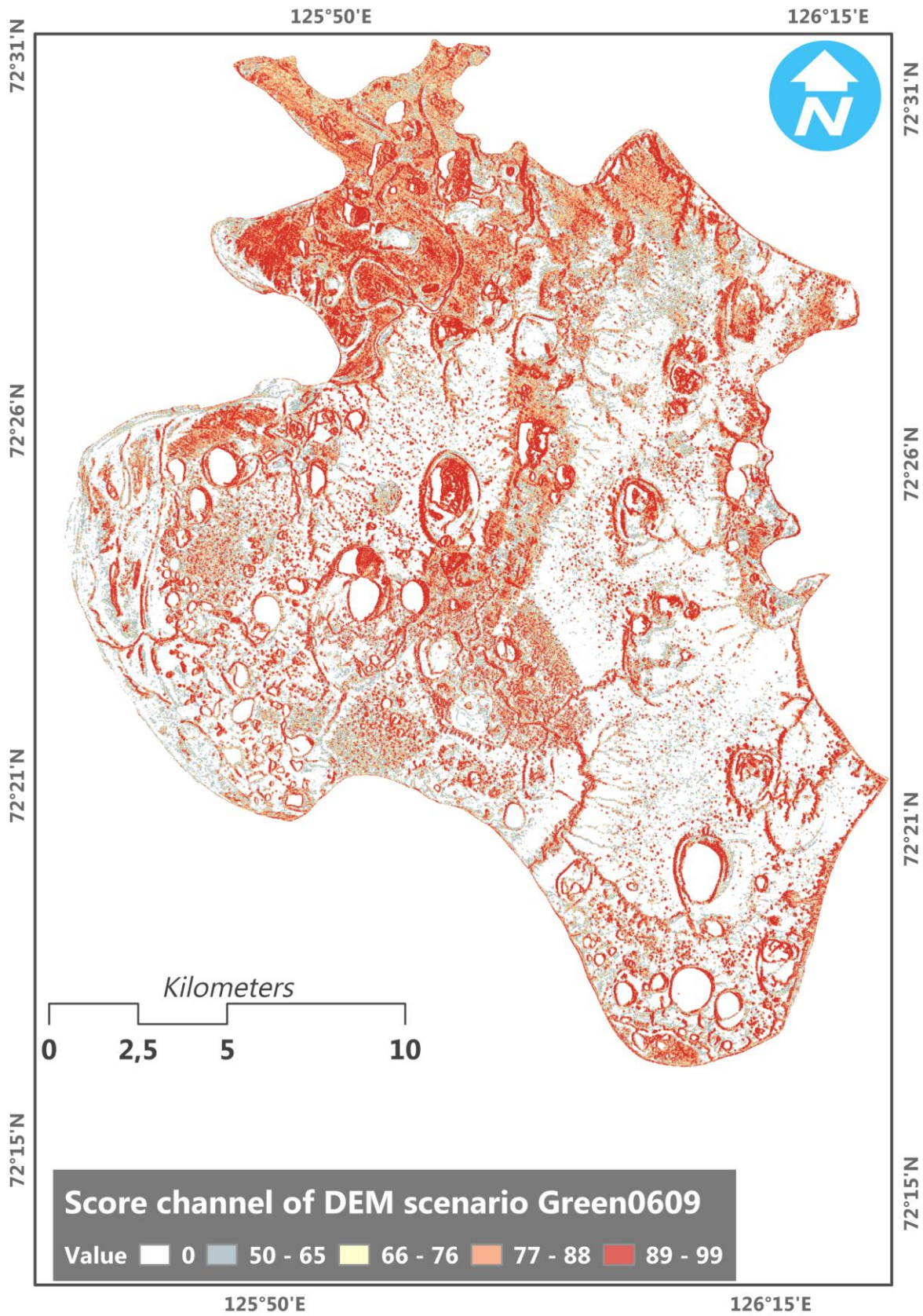
Figure 5-6: Score channel results for DEM scenario Green0609. White color indicates areas that could not be correlated during image matching and are interpolated in the DEM.

5.2   Stream network

The stream network of Kurungnakh Island shows four levels of stream ordering (Figure 5-7). The majority of the stream links (71%) are of first order with a total length of 244 km (Table 5-2). Of these streams 49 % are classified as thermokarst affected. Streams of first order occur all over the island, at slopes of thermokarst depressions or alasses, on Ice Complex surfaces and on the coastline to the Lena River Delta channels. About a fifth (18 %) of the stream links has a stream order class of 2 and a total length of 54 km. Of these 42 % are classified as thermokarst affected. They occur on various sites all over the island but tend to be located more on the lower slopes of thermokarst depressions and are often connected to thermokarst lakes or drained thermokarst lakes. In the northern part of the study area streams with an order of 2 can be observed that occur on the Ice Complex surface. Streams with a stream order of 3 make up 8% of all stream links and have a total length of 28 km. Of these 33 % are situated in thermokarst affected areas. Most of the streams with this stream order are connected to thermokarst lakes, but there are few stream links that occur without the presence of thermokarst lakes, for example in the northwestern part of the Ice Complex extent of Kurungnakh Island.

Three stream systems with a stream order of 4 with a total length of 10 km are detected. Only 9 % of the stream links of this stream order are located in thermokarst affected terrain. Two stream systems of order 4 are connected to the main alas valley in the center of the island, while the third that develops over a short distance is located at the northern part of the island, where it cuts the Ice Complex extent before it enters the Lena River Delta channel. The total length of stream links decreases with increasing stream order, while the mean stream link length slightly increases, except stream order 2. The percentage of stream links in thermokarst-affected terrain decreases with increasing stream order.

Table 5-2: Characteristics of the stream network of Kurungnakh Island.

Stream order	No. of stream links	Percentage of stream links	Cumulated stream length [km]	Mean stream link length [m]	Streams in thermokarst depressions [%]
1	861	71	244	283	49
2	222	18	54	241	41
3	98	8	28	291	33
4	33	3	10	317	9
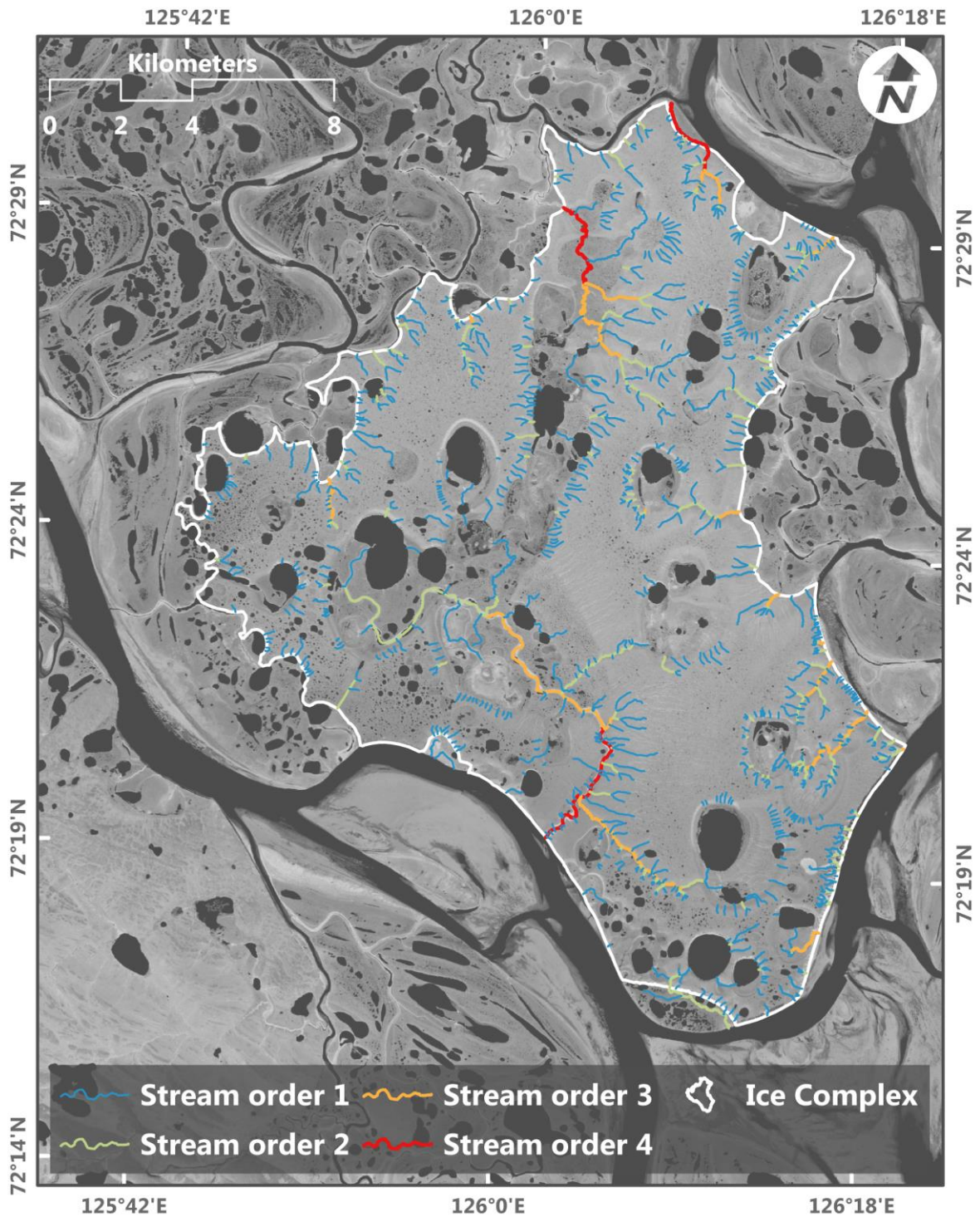
Figure 5-7: Strahler stream order for the stream network of Kurungnakh Island within the Ice Complex extent. Background image: RapidEye, band combination 5, 5, 5; projection UTM Zone 52N within WGS 84 datum.

The stream network can be divided in two main sections. Complex stream systems, as expressed through a higher stream order, are observed within the wide alas valley in the central part of Kurungnakh Island. Here streams of lower order, which have their origin on the Ice Complex surface, coalesce to higher order streams before they exit the Ice Complex.

Within the central alas valley the northern streams follow the general height gradient towards northwest, while the southern streams are draining in southeast direction.

On the higher elevated Ice Complex surface that is not affected by thermokarst, fewer streams occur that are predominantly of first or second order. If the Ice Complex surface is degraded by thermokarst, streams of higher order occur that connect the thermokarst lakes with the Lena River Delta channels.

5.3 Orientation of stream links

Figure 5-9 shows the stream links that were used for orientation analysis. A differentiation of stream links within and outside of thermokarst depressions was performed since they have different characteristics, as figure 5-8 shows. While the majority of stream links in thermokarst depressions are mostly concentrated in the alas valley area and in the southeast of Kurungnakh Island, the stream links outside of thermokarst depressions are well distributed all around the study area and predominantly connect the study area with the Lena River Delta channels in the northeast, south and southwest, or with the first terrace in the east, and west to northwest (Figure 5-9). Exceptions are the stream links in the "Main Valley" area that are situated more inland. Figure 5-8 shows the frequency distribution of stream link lengths and the direction of stream links within thermokarst-affected terrain (blue) and outside of thermokarst-affected terrain (green).
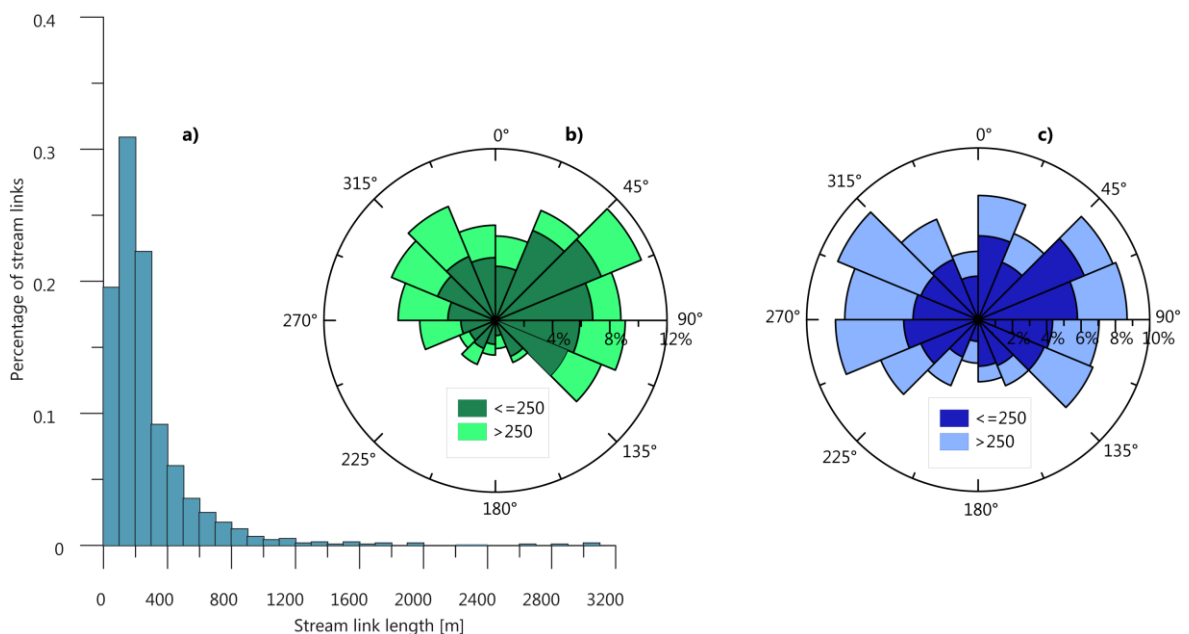
Figure 5-8: Directions of stream links: a) frequency distribution of stream link length in %; b) orientation of stream links [°] located outside of thermokarst depressions and stream link length [m]; c) orientation of stream links [°] within thermokarst depressions and stream link length [m]. Values in diagrams b and c were bundled to classes of 22.5 degrees. Consider the different scales in the radius axis.

37
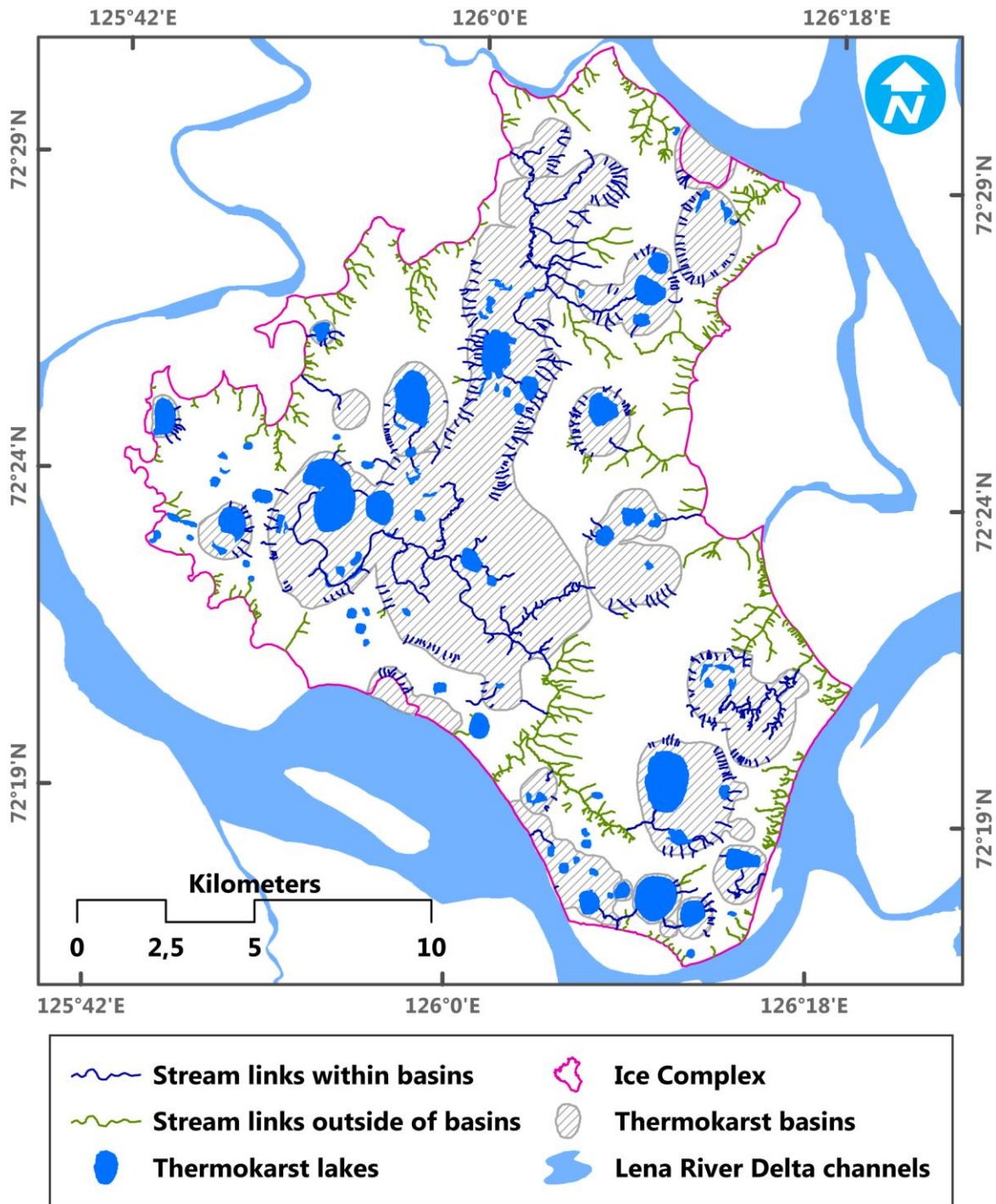
Figure 5-9: Stream links of Kurungnakh Island within (blue) and outside (green) of thermokarst affected terrain.

In total 1214 stream links were analyzed ranging from 4 to 3078 meter length and having a mean length of 277 meter. 63% of these stream links are shorter than 250 m. Stream links within thermokarst-affected terrain show a strong east-west distribution with a small tendency of stream links longer than 250 m towards the east and shorter stream links towards the west. While there is a small peak of 8% between 0° and 22.5°, the southern directions between 135° and 225° make up only minor portions.

Stream links outside of thermokarst depressions show a more consolidated distribution. Most of the stream links have direction towards east with a small peak of about 11% of all streams towards 45° to 76.5 °. Another portion of the streams shows northwestern directions between 270° and 337.5°. Smaller stream links tend to the eastern directions.

5.4 Transversal profiles

The profiles in the "Drained Lake Valley" are mostly v-shaped with a clear visible stream center, except profile TP 05 which has a u-shape and a wider floor (Figure 5-10). The slope of the valleys is decreasing with distance from the coastline. The deepest profile with 39 m incision is TP 02. TP 05 has the highest observed slope with 30.12° (Table 5-3). TP 04 shows two depressions because it ranges over two small gullies.

Profiles extracted from the DEM do reflect the actual morphology, except at TP 03 and TP 04. DEM values of TP 03 show an inverted shape compared to the field data and actual terrain is overestimated. TP 04 is u-shaped in DEM values while actual topography shows a v-shape. The DEM values of TP 02 and TP 05 are both overestimating heights on the terrain surface and underestimating the valley floor. Mean slopes extracted from the DEM show a mean difference of about 7° from the actual mean slope (Table 5-3).

Table 5-3: Morphometric characteristics of transversal profiles in the "Drained Lake Valley".

Profile ID	Length [m]	Depth [m]	Slope left [°] Field data	Slope left [°] Raw DEM	Slope right [°] Field data	Slope right [°] Raw DEM	Slope difference [°] left	Slope difference [°] right
TP 01	171	22	14.67	12.37	14.12	11.77	2.30	2.35
TP 02	254	39	18.27	15.76	16.62	15.62	2.52	1.00
TP 03	32	2	6.70	2.05	5.56	-0.51	4.66	6.07
TP 04	73	6	13.26	4.19	7.96	3.48	9.08	4.48
TP 05	125	31	30.12	21.65	25.61	21.82	8.47	3.78
					Mean		7.04	6.43
					SD		6.92	5.58

Figure 5-10: Map and plots of transversal profiles in the "Drained Lake Valley" study site. Positions of the profile lines in the graph correspond to the position in the map. Lines show the profiles from the RTK survey while the dashed lines show the values extracted from the raw DEM. Background image: GeoEye-1, band combination 3,3,3.
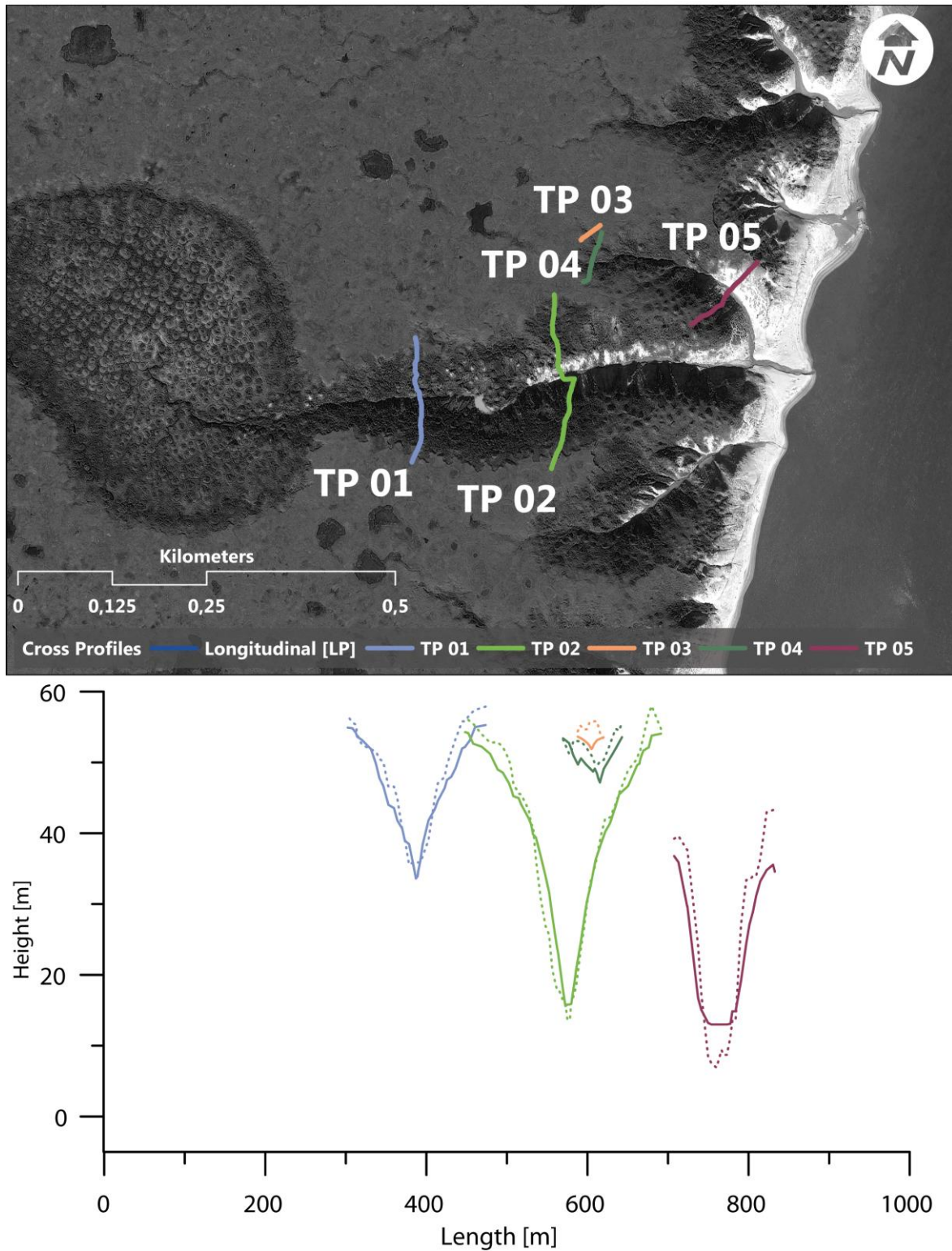
The transversal profiles of the "Lucky Lake Valley" shown in figure 5-11 can be divided in three sections: 1) the upper catchment with profiles TP 01 - TP 04 and TP 12; 2) the middle catchment with profiles TP 05 – TP 09; and 3) the lower catchment with profiles TP 10 and TP 11. There morphometric characteristics are shown in table 5-4.

The profiles in the upper catchment of the "Lucky Lake Valley" have gentle slopes with convex character. TP 01, located near to the outflow of the "Lucky Lake", has a wide and flat floor. TP 02 is located directly below a drained thermokarst lake in a small tributary of the "Lucky Lake Valley" and has gentle slopes and a flat bottom. TP 03 shows a very symmetrical profile and has a visible stream center, while TP 04 features a terrace in the valley floor and is asymmetrical shaped. It marks the transition from the upper catchment within the Ice Complex to the middle catchment that belongs to the first main geomorphological terrace of the Lena Delta.

All profiles of the "Lucky Lake Valley" middle catchment show a u-shaped, terraced form with an incised stream center. TP 06 is most characteristic for this shape. Profiles TP 05 and TP 07 are located in bends of the stream, are narrower than TP 06 and have an asymmetric shape. In profiles TP 08 and TP 09 have the clearest asymmetry due to a terrace on the right side of the profile.

TP 10 finally belongs to the lower catchment of the "Lucky Lake Valley" at the mouth of to the Lena River Delta channel and is v-shaped. TP 11 has a v-shaped and narrow geometry, characteristic for short gullies that deeply incise into the surface.

Table 5-4: Morphometric characteristics of transversal profiles in the "Lucky Lake Valley".

Profile ID	Length [m]	Depth [m]	Slope left [°]		Slope right [°]		Slope difference [°]	
			Field data	Raw DEM	Field data	Raw DEM	left	right
LLV TP 01	319	19	6.26	5.85	7.28	6.23	0.41	1.04
LLV TP 02	168	4	2.63	5.03	3.36	1.48	-2.40	1.88
LLV TP 03	264	20	8.96	6.42	8.06	7.14	2.54	0.93
LLV TP 04	267	21	9.69	9.42	8.10	9.06	0.26	-0.96
LLV TP 05	36	5	16.84	-1.37	14.50	5.20	18.21	9.31
LLV TP 06	43	6	16.51	2.85	15.62	5.62	13.66	10.00
LLV TP 07	66	6	12.90	10.79	7.40	1.16	2.11	6.24
LLV TP 08	70	8	8.77	1.79	20.39	12.94	6.98	7.44
LLV TP 09	64	9	14.58	7.29	16.11	8.36	7.29	7.75
LLV TP 10	67	9	14.75	-1.76	14.45	6.51	16.51	7.94
LLV TP 11	25	6	24.05	-2.09	28.19	5.56	26.15	22.63
LLV TP 12	162	7	4.56	4.58	5.16	4.20	-0.03	0.96
					Mean		7.64	6.26
					SD		9.01	6.42
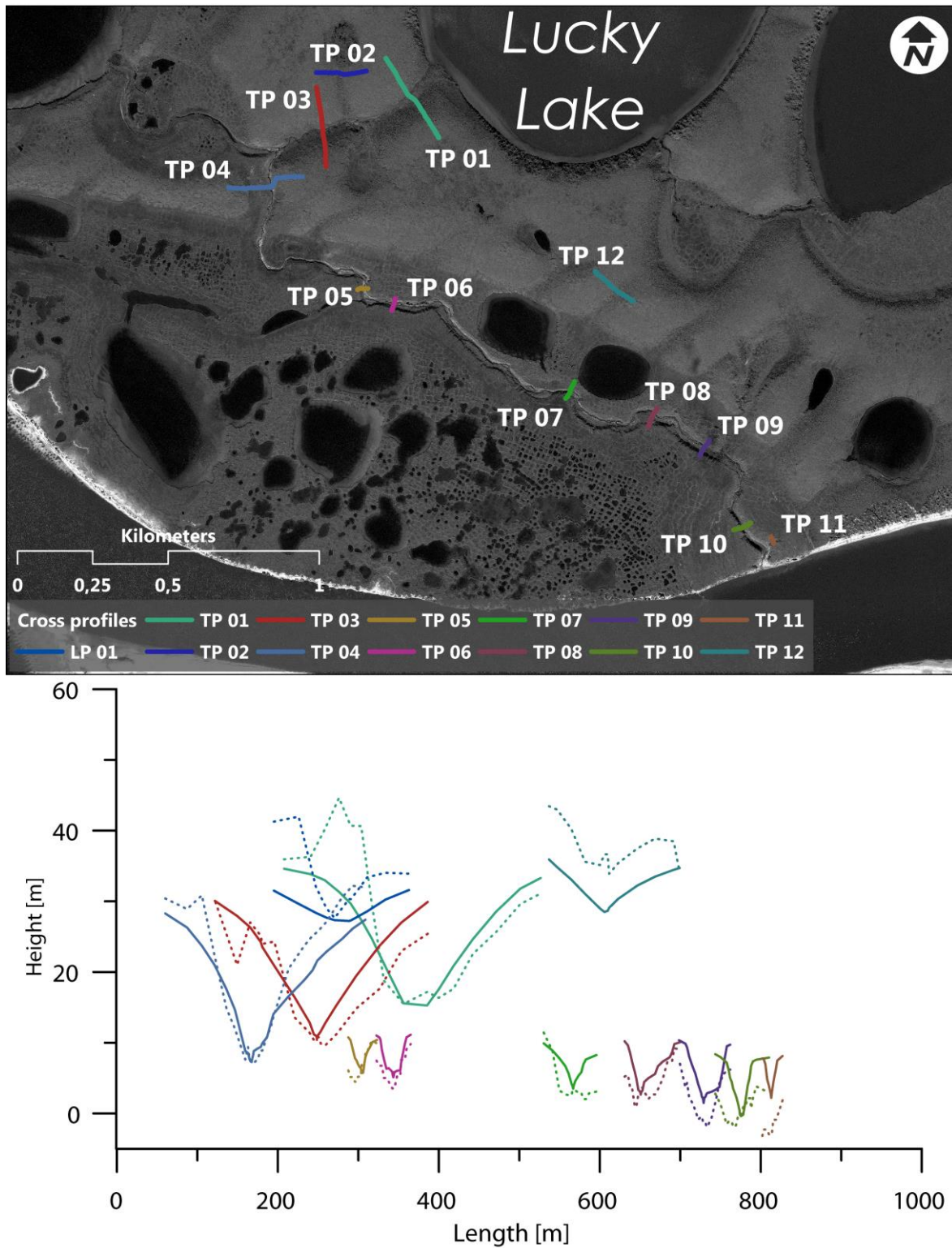
Figure 5-11: Map and plots of transversal profiles in the "Lucky Lake Valley" study site. Positions of the profile lines in the graph correspond to the position in the map. Lines show the profiles from the RTK survey while the dashed lines show the values extracted from the raw DEM. Background image: GeoEye-1, band combination 3,3,3.

The DEM derived profiles reflect the actual valley morphology in most cases, but the terrace form is not as clearly visible as it is in the field data. The DEM extracted profile TP 03 is showing a slightly different shape than the field data, with a wide floor und concave slope

and DEM extracted TP 01 has an artificial peak on the left side of the profile. TP 02 has a gentle profile u-shape, while the DEM profile line is showing a more v-shaped valley with a high slope on the left side of the profile. Profile TP 11 is completely different in shape and height. TP 10 is wider and not as deeply incised as the actual profile line. TP 08 shows an inverted stream center. TP 09 is reflecting general morphology, but is missing the terrace and has a shift in y-direction of about 4 m.

The morphometric properties of the profiles are basically reflected in the DEM, mean difference of slope is 7.64 for the left side of the profiles and 6.26 on the right side of the profiles. The transversal profiles TP 05, TP 06. TP 10 and TP 11 show the highest slope deviations compared to the field dataset (Table 5-4).

The transversal profiles of the "Main Valley" (Figure 5-12) can be divided into three sections: 1) the main distributary (TP 03, TP 07 and TP 09); 2) the long tributaries (TP 01, TP 02, TP 04 and TP 05); and 3) the short tributaries (TP 06, TP 08, TP 10 and TP 11). There morphometric characteristics are shown in table 5-5.

Profiles TP 03, TP 07 and TP 09 are located in the main distributary that has very gentle slopes as observed through the lowest points of the previously mentioned profiles. TP 03 shows an asymmetric shape and is S-N orientated with a terrace at about 5 MASL on the southern side. In TP 07 the terrace is not strongly developed and is symmetric. TP 09 shows a second terrace at about 15 MASL on the northeast facing side. The stream channel in the distributary is well developed and up to ten meters wide.

Table 5-5: Morphometric characteristics of transversal profiles in the "Main Valley".

| Profile ID	Orientation [°]	Length [m]	Depth [m]	Slope left [°]		Slope right [°]		Slope Difference [°]	
				Field data	Raw DEM	Field data	Raw DEM	left	right
MV TP 01	28	133	2	1.29	0.23	2.75	-1.75	1.06	4.49
MV TP 02	46	80	3	4.10	0.93	4.95	3.12	3.18	1.84
MV TP 03	6	146	11	8.43	4.51	8.15	4.46	3.92	3.69
MV TP 04	35	99	10	15.31	9.75	7.84	3.27	5.56	4.56
MV TP 05	98	69	10	16.65	4.89	17.87	-2.88	11.77	20.75
MV TP 06	84	46	5	9.25	1.90	12.33	2.61	7.35	9.72
MV TP 07	127	121	12	12.43	4.76	9.91	2.97	7.67	6.95
MV TP 08	24	45	5	17.44	8.32	10.20	2.87	9.13	7.33
MV TP 09	64	159	12	6.18	3.37	12.83	7.96	2.81	4.87
MV TP 10	50	70	6	6.93	2.96	11.52	3.38	3.97	8.15
MV TP 11	79	44	8	26.91	4.94	16.64	1.63	21.96	15.01
							Mean	7.13	7.94
							SD	5.93	5.76
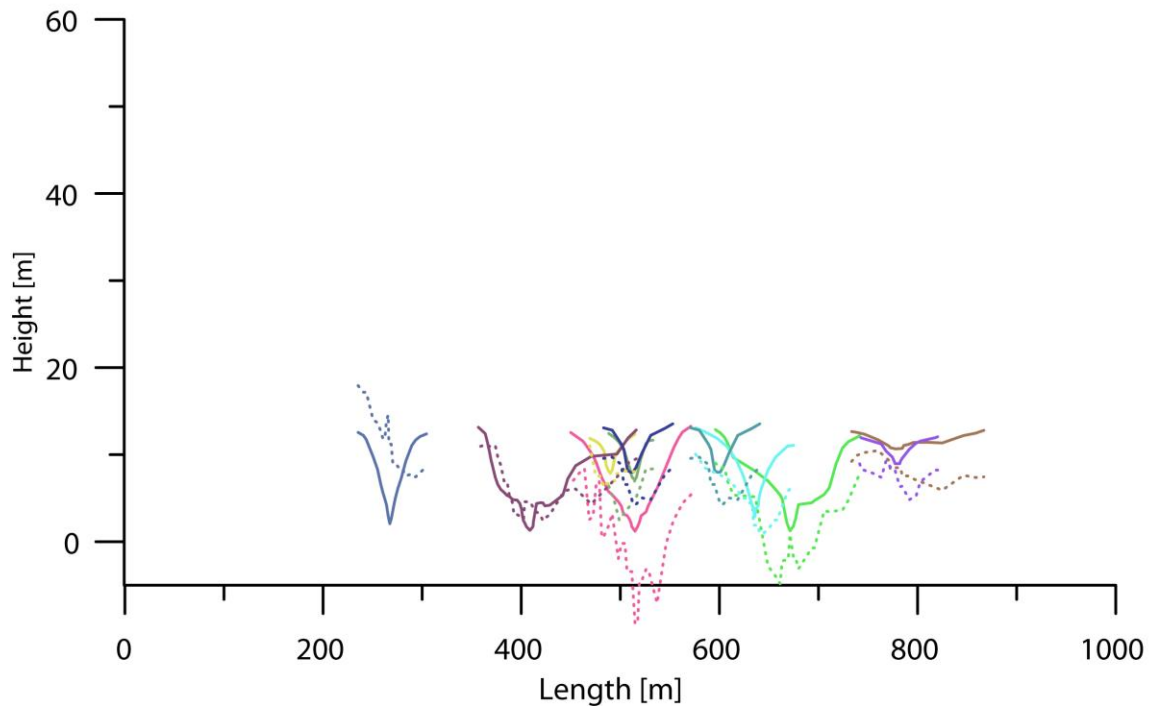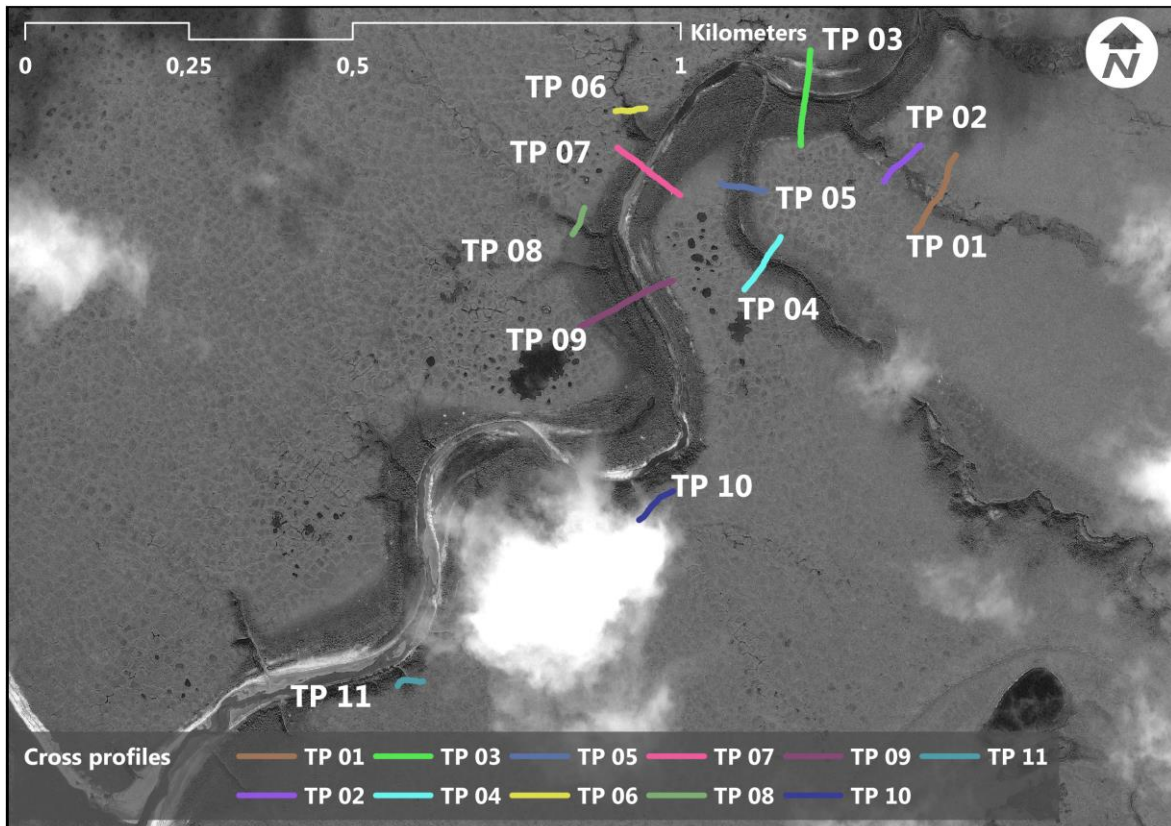
Figure 5-12: Map and plots of transversal profiles in the "Main Valley" study site. Positions of the profile lines in the graph correspond to the position in the map. Lines show the profiles from the RTK survey while the dashed lines show the values extracted from the raw DEM. Background image: GeoEye-1, band combination 3,3,3.

The profiles of the long tributaries feature diverse shapes. TP 01 is very flat and with gentle slopes and shows a flat bottom without a distinct stream center. TP 02 is incised

several meters in a v-shaped form but with a flat bottom and gentle slopes. TP 04 has a v-shaped form with steep slopes in the bottom but with stilted more gentle slopes towards the surface. TP 05 is v-shaped with steep slopes and has a flat surface. TP 04 and 05 are incised to about 10 m; TP 02 is only incised to about 3 m.

The profiles of the short tributaries are predominantly v-shaped, with a flat floor and gentle slopes on the terrain surface. TP 11, located nearly at the mouth to the Lena River Delta channel, has slightly higher slopes and is not showing a flat bottom. The terrain heights of the transversal profiles in the "Main Valley" study site do not exceed 15 MASL.

The morphology of the transversal profiles is partly reflected by the DEM, but the extracted profiles in the "Main Valley" show a general underestimation of actual heights as well as planimetric shifts in some cases. In TP 03 and TP 09 the stream center of the DEM extracted profiles is inverted. In TP 07 the wavy noise of the DEM is visible on the left side of the profile. The mean slope differences are 7.13° and 7.94° for the left and right transversal profiles side, respectively.TP 05 and TP 11 show the highest deviations compared to the field dataset (Table 5-5).

5.5 Longitudinal profiles

Figure 5-13 shows longitudinal profiles of the "Lucky Lake Valley" and "Drained Lake Valley". The morphometric characteristics of the profiles are presented in table 5-6. The LLV LP 01 has a length of 3 204 m and height decreases by 16.49 m from highest to the lowest point with a mean slope of 0.51°. The profile can be divided in two parts. At the beginning of the profile the line has a slightly higher slope than at its end. The break line of slope change is at 743 m in x-direction. After this point the profile is slightly decreasing towards the mouth to the Olenyokskaya Channel.

Table 5-6: Morphometric characteristics of longitudinal profiles in the three key sites. Profiles with the rDEM appendix are extracted from the raw DEM.

Profile ID	Highest point [MASL]	Lowest point [MASL]	Height difference [m]	Length [m]	Slope [°]
LLV LP 01	16.25	-0.23	16.49	3204.09	0.29
LLV LP 01 rDEM	18.65	-1.29	19.94	3204.09	0.36
DLV LP 01	48.85	4.89	43.96	1059.27	2.38
DLV LP 01 rDEM	51.91	2.89	49.02	1059.27	2.65
MV LP 01	14.21	1.65	12.57	146.64	4.90
MV LP 01 rDEM	13.27	-1.18	14.46	146.64	5.63
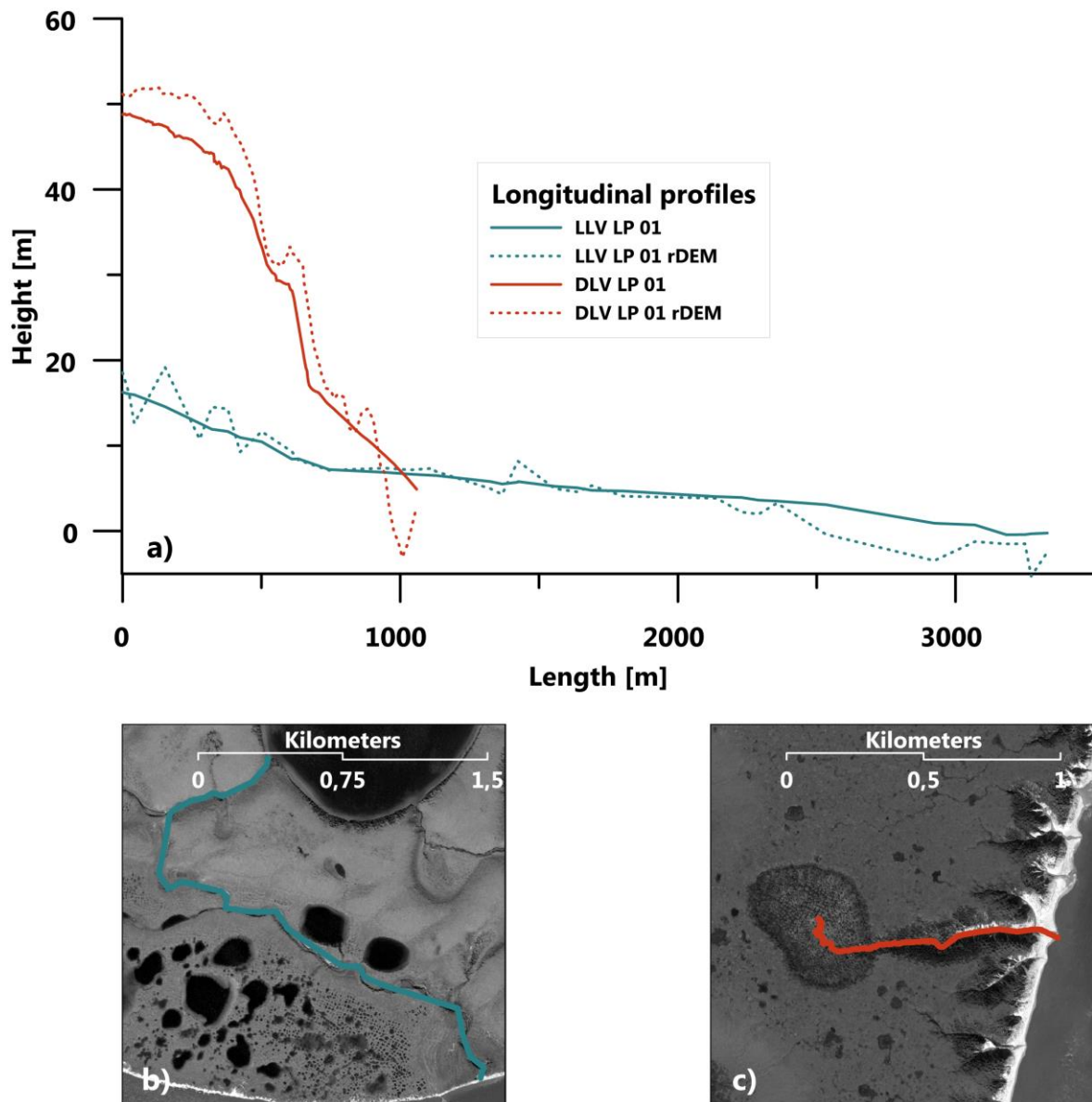
Figure 5-13: a) Longitudinal profiles of the b) "Lucky Lake Valley" and c) "Drained Lake Valley" study sites. Lines in a) show the profiles from the RTK survey while the dashed lines show the values extracted from the raw DEM.

The profile line from the DEM is generally reflecting the shape of the profile from the RTK GPS survey. In the upper part of the profile some parts are overestimated and in the lower part the actual profile line is underestimated. The mean slope of 0.36° is just slightly differing from the RTK profile value of 0.29° (Table 5-6).

Profile DLV LP 01 can be divided in four parts. In the beginning the slope is relatively gentle up to circa 400 m before the profile line gets steeper. At about 600 m a small plateau is visible after which the profile shows the steepest part up to about 700 m. The last part of the profile shows a gentler slope.

The values of the DEM are reflecting the actual morphology of the profile. In the first part of the profile the heights are overestimated by the DEM, while in lower part the dotted line

shows a notable underestimation of actual terrain height. The mean slope of the DEM profile line of 2.65° is just slightly higher than the actual slope of 2.38° (Table 5-6).

Table 5-7: shows statistical parameters of the comparison of slopes from the RTK survey to the DEM scenario Green0609 for 833 values. These values were calculated on the basis of the RTK GPS points that were taken in the field at significant changes of topography (Figure 4-6 in chapter 4.6). Mean deviation of slope is 11.9° with a standard deviation of 14.85°.

Table 5-7: Evaluation results of slope accuracies for scenario Green0609. Values of the RTK measurements were compared to the values extracted from the DEM. Values with slopes over 90° were excluded from the calculation, because they were observed at points with very short distance and resulted in unrealistc values.

Parameter	Value
Number of records	833
Mean deviation	11.90
Median of deviations	6.03
Standard Deviation	14.85
Minimum	0.00
Maximum	90.52

6   Discussion

6.1   DEM accuracy and valley morphometry

The results in chapter 5.1 show that the use of more images than the generic triplet within the DEM generation process can improve the vertical accuracies of the resulting DEM. But this is just valid for scenario Green0609. Scenario allc0609 for instance, which used the most stereopairs showed only the fifth highest accuracies. Scenarios that include stereopairs with a B/H ratio that possibly exceeds a value of 1 (scenario Greenred06) showed a low DEM accuracy, therefore these scenarios are not recommended for DEM extraction. Similar effects are also reported by *Hasegawa et al.* [2000] and *Raggam* [2006]. A significant increase of the mean score channel value or the percentage of correlated pixels could not be observed when consolidating the data by adding more images to the DEM generation process (Table 5-1).

The vertical accuracies of 4.41and 4.92 MASL for the final DEM scenarios Green0609 and Triplet, respectively, are in the range of other reports that evaluated PRISM derived DEMs [*Bignone and Umakawa*, 2008; *Gruen and Wolff*, 2007]. Depending on the planned application of the DEM, one could avoid the time exposure of processing additional images, including GPC search and computation time, if a slightly improved vertical accuracy of 0.5 m is not necessarily needed.

Two different editing approaches were applied to the final DEMs (Figure 6-1). Associated with the editing process some compromises had to be made regarding the accuracy.
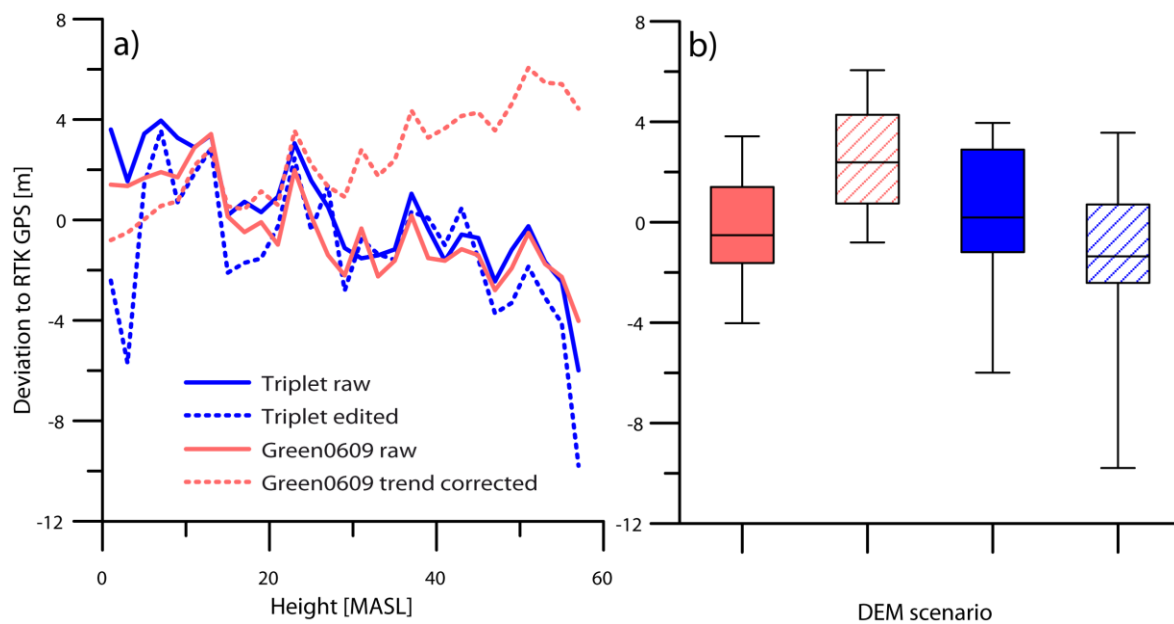

Figure 6-1: DEM error estimations and relief height before and after editing: a) deviations of scenario Green0609 and scenario triplet with 5x5 meter ground sampling distance related to the terrain height. b) solid filled and forward-slashed filled box-whisker plot represents the raw and the edited DEM respectively. The color code corresponds to diagrams a) and b).

The use of a linear trend surface on the scenario Green0609 DEM based on the mean classified deviations to the RTK GPS values results in a positive shift of mean deviations of about 2 MASL without a significant change in the variance of the deviations (Figure 6-1 b) and Table 6-1). Consequently the DEM is predominantly underestimating actual terrain heights (Figure 6-1 b). This effect increases with increasing absolute terrain height. The editing of scenario Triplet is decreasing the mean deviations from 0.27 MASL to -1.17 MASL whereas the variance is increasing from 5.30 to 7.50 MASL. This effect can be observed at the upper and lower ends of the absolute height range of Kurungnakh Island where the edited DEM overestimates the actual terrain heights. For the low lying areas, this is mainly due to the filling of sinks in the DEM that occur especially in the "Main Valley" site with low absolute relief heights. Concluded, the editing process may lead to a smoothed surface that contains less noise, but vertical accuracies in low and high laying areas decrease.

In all DEM scenarios large percentages of non-correlated pixels could be observed with values ranging from 42.83% to 71.02%. As shown in figure 5-6, the areas that could not be correlated during image matching are predominantly located on undisturbed and flat Ice Complex surfaces. Interpolation is used to attain elevation values for these areas. This is sufficient when there are no great height differences and some small features are present that could be matched and deliver spot-like height information. But on the large west to southwest facing slopes from the Ice Complex surface towards the central alas valley where in some regions no matching features occur, the results of the interpolation are uncertain and should be dealt with carefully when using the produced DEM. Using tachymetry or RTK GPS, small-scale and high-resolution DEMs should be created for these low contrast slope areas to evaluate the quality of the DEMs. Therefore, further survey campaigns should be conducted to validate these areas and to consolidate the existing GCP network that now span to the three key sites of this work. These surveys should be connected to the existing GCP network that is used for DEM generation, so that a comparison of absolute heights is possible.

Table 6-1: Statistical characteristics of height deviations compared to the RTK GPS measurements for scenarios Green0609 and Triplet before and after using two editing approaches. Values are given in MASL.

	GREEN0609 Raw	GREEN0609 trend corrected	Triplet raw	Triplet edited
Standard deviation	1.82	1.92	2.30	2.74
Mean	-0.40	2.48	0.27	-1.17
Median	-0.52	2.39	0.19	-1.36
Minimum	-4.02	-0.80	-5.99	-9.79
Maximum	3.42	6.06	3.96	3.56
Variance	3.31	3.68	5.30	7.50

The sharp height deviation step at about 12 to 14 MASL that occurred in all DEM scenarios during evaluation is a striking feature that needs explanation. The RTK GPS measurements itself that were used for evaluation could be the reason for some irregularities in the evaluation process. The three study sites were too far away from each other to use only one base station for all measurements. Thus three base stations had to be set up. The relative accuracies of the RTK-GPS measurements of one survey may be in centimeter level, but the absolute height can vary in a range of 1 to 2 MASL for the same base station between different days of observation and to a maximum of about 3 MASL between different base stations and survey days (Table 6-2). These differences in between different observation days could have an impact on the evaluation, but do not fully explain the deviation step that is in a range of up to 8 MASL.

The shape of transversal and longitudinal profiles is reflected by the produced DEM in most cases. Extracted profiles from areas outside of the three study sites could be used to further analyze the stream network. Still some differences have to be taken into account when analyzing profiles that were extracted from the DEM. The raw DEM tends to over-estimate or underestimate actual terrain heights below 15 MASL and over 20 MASL, respectively. Therefore, the valley shape may be drawn correctly but absolute heights can vary in both directions of the y-axis. As clearly visible for TP 03 within the "Drained Lake Valley", short transversal profiles on Ice Complex surfaces are susceptible for errors, because the resolution of the DEM is not sufficient to describe small scale features with only few meters of incision. Extracted transversal profiles in "Main Valley" showed inverted shapes in the stream center (Figure 5-12) because of matching difficulties of the PRISM dataset in low lying areas. While the terraces in the "Drained Lake Valley" are only rudimentary expressed in the DEM extracted profiles, the wider terraces in the "Main Valley" are well represented in the DEM derived profiles. V-shaped ravines or valleys are well reflected by the DEM.

Table 6-2: Height differences of RTK GPS base stations. Reported heights origin from device records and field book entries from different observation dates

	KURBASE1 (LLV)	KURBASE2 (MV)	KURBASE3 (DLV)
Reported height [MASL]	27.46	6.38	46.19
Reported height [MASL]	29.33	7.56	45.90
Reported height [MASL]	29.32	6.99	45.90
Reported height [MASL]	29.46		46.97
Standard deviation	0.95	0.58	0.50
Variance	0.91	0.34	0.25
Range	1.99	1.17	1.07

The DEM derivate slope showed different results for different scales. The comparison of small scale slope values from the RTK GPS and the DEM showed a mean deviation of 11° for all investigated profiles. When using the mean slope of a profile, based on its highest and lowest point, the mean deviation for the profiles in the three study sites ranged only between 6.9 to 7.9°. The three analyzed longitudinal profiles showed an even lower deviation of below 1°. The use of PRISM derived DEMs for analysis of first order morphometric derivate slope is sufficient when using the mean value of a profile. Longitudinal profiles are possibly better reflected by the DEM as transversal profiles but should further be evaluated.

6.2   Stream network evolution

The stream network within the Ice Complex of Kurungnakh Island can be divided in two main parts. These are the ones that are situated within and outside of thermokarst affected areas respectively. More complex structures occur mostly on alas floors, where also meandering stream links can be observed, while the transition zone from the Ice Complex surface to the alas bottom is characterized by the presence of lower order streams with short and straight character. The stream network shows a stage of high organization in three spots around the study area. Two of them are situated in thermokarst depressions with low elevations where flowing water from adjacent surfaces concentrates and consequently forms advanced networks.

Of particularly interest in this context is the stream on the northern edge of Kurungnakh Island that has a stream order of 4. It is neither situated in an alas depression nor connected to a big thermokarst lake but nevertheless incised into otherwise undisturbed Ice Complex deposits. On relatively short distance a high degree of organization is developed in this stream that expresses itself through an early stage of dendritic form. The Lena River Delta channel that erodes the cliff is probably the main driver for the occurrence of this feature, because the base level of erosion is constantly changing.

Furthermore streams can be distinguished between those that are located on the outer extent of Kurungnakh Island and the ones in the inland. In the first case the Lena River Delta channel is an important thermo-erosional factor that again has a substantial influence on the development of thermo-erosional valleys on land. Thermo-erosional riverbank erosion, alters the base level of erosion and promotes a faster development of thermo-erosional valleys with high erosional activity due to constant high slope gradients. Accompanying with the height gradient of Kurungnakh Island, the most prominent representatives of this valley type occur at the eastern shoreline of Kurungnakh Island in the area of the "Drained Lake Valley". With the exception of the southwestern shoreline around the "Main Valley", these streams occur all

around the margins of the study area. This is also expressed through the orientation analysis in figure 5-8.

The intense thermokarst activity that lead to the formation of the wide alas valley is an important factor in the evolution of the stream network of Kurungnakh Island. The obvious coalescence of several thermokarst depressions that form the valley corresponds to stage 4a of the alas relief development by *Soloviev* [1973] (Figure 2-9).and represents a late stage of permafrost degradation. Today the alas valley is divided into two parts that drain in opposing directions. The northern part is following the general height gradient and drains towards northeast. The southern part is first draining in southeast direction, before it takes a nearly rectangular turn within Ice Complex deposits and enters the delta channel in southwestern direction. The neo-tectonic activity in the Lena River Delta that changed flow directions of the major delta channels in the past could also have had an impact on the smaller scale stream network on Kurungnakh Island.

The general height gradient of Kurungnakh Island towards northwest is also a main driving factor for the direction of detected streams and was identified in the mean directions of stream links. The influence of thermokarst features is superimposing this signal due to partly radially structured short and straight streams that occur on the slopes of the thermokarst depressions. Also the streams at the margins of Kurungnakh Island show a very heterogeneous orientation. In the "Main Valley" that is N-S orientated the resulting short and straight gullies are consequently perpendicular orientated in East and West directions.

Polygon nets in the ground can vary in their structure and not necessarily have a hexagonal structure with angles of 60°. The identified peaks of directions of the stream links could therefore follow the polygonal net structure, but are more likely influenced by the main topographic properties of the study area. This is because the stream link dataset is not necessarily representing every bend of a stream. Future works should identify stream segments between every bend of a stream and analyze the directions of these segments to verify the hypothesis that stream segments are orientated according to the polygonal net.

6.3 Valley morphometry

The three observed study sites show different valley geometries and characteristics. While the "Drained Lake Valley" features predominantly sharp v-shaped valleys that are incised up to 40 m into the Ice Complex, the main characteristics of the "Lucky Lake" are a u-shaped form of the profiles with a terraced valley bottom (Figure 6-2). The transversal profiles of the "Main Valley" finally show wider and gentler slopes and incorporate two terraces in some profiles.
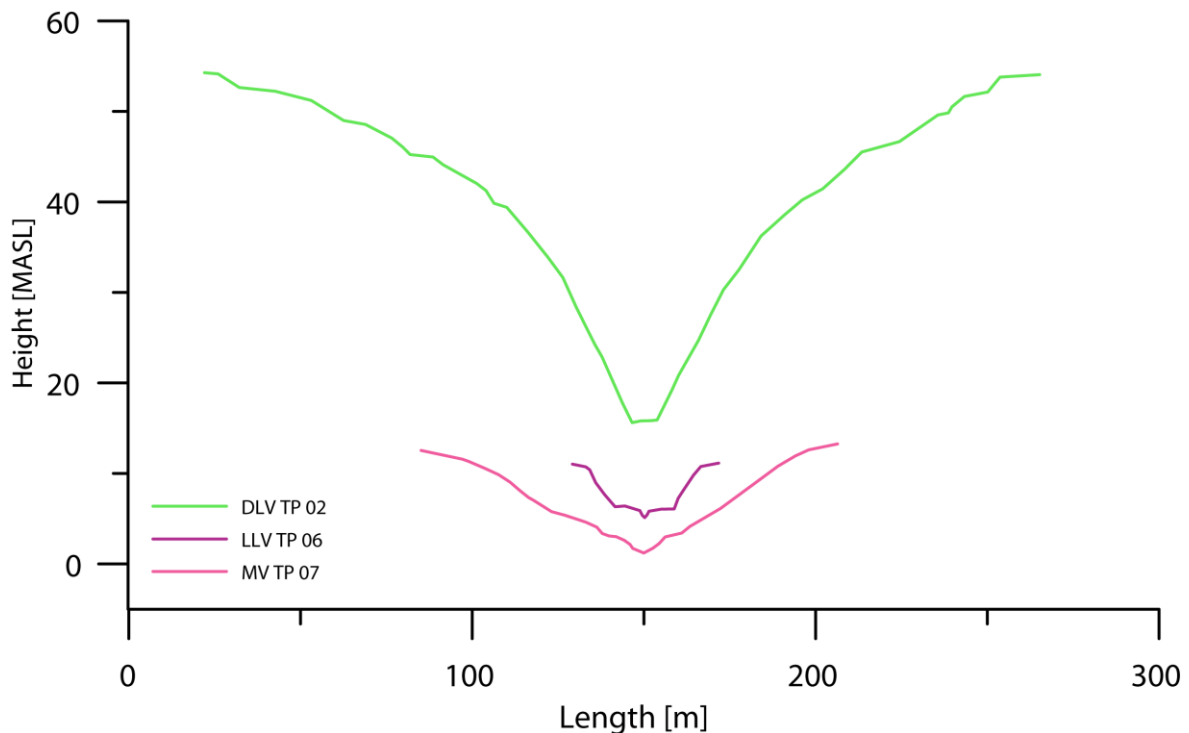
Figure 6-2: Comparison of transversal profiles from the three key sites.

Particularly the morphometry of the longitudinal and transversal profiles within the "Drained Lake Valley" is worth to be emphasized because it results from the combination of three different processes: 1) vertical thermal erosion that follows the high height gradient from the surface to the coastline; 2) lateral thermal erosion at the base level from the Lena River Delta channel; and 3) a draining event of a thermokarst lake. Draining events of thermokarst lakes occur throughout the Arctic as a result of mainly lateral drainage due to bank overflow, ice wedge degradation and development of a drainage network, headward stream erosion, lake tapping, coastal erosion, as well as expansion of a lake toward a drainage gradient [*Jones et al.*, 2011]. In the case of the "Drained Lake Valley" it is very likely that the combination of retrogressive erosion of the thermo-erosional valley that followed the lateral thermal-erosion by the Lena River Delta channel and bank overflow of the lake in seasons with high water availability triggered the drainage of the thermokarst lake [*Morgenstern*, 2012]. This event happened after 1964 as Corona satellite images show.

The transversal profiles in the "Lucky Lake Valley" reflect the transition from the Ice Complex of the third terrace to the active floodplain system of the first terrace. Especially the detected terraces are a striking feature. These are mostly located on the southern side of the profiles and lead to more gentle slopes, while steeper slopes occur on the southwest facing side of the profiles. Snow is mainly accumulated on the southern side because it is protected from the prevailing wind direction from south [*Morgenstern et al.*, 2011]. As mentioned, snow patches could have a substantial impact on the valley evolution since they are eroding the

underlain surface when melting in summer and accumulation of fine material from eolian input remains. Most likely the terraces are composed of a mixture from these materials as well as from the fine-grained sediments from the eroded Ice Complex deposits transported downstream and from fine material transported upstream by the Lena River during flooding events.

Because of its constant low heights, the "Main Valley" is as well very likely influenced by major flooding events of the Lena River that can occur every year in spring during ice break up. They can reach high levels, as drift wood findings during the field campaign in the "Main Valley" area at 11 MASL indicated (Figure 6-3).

Figure 6-3: Historical drift wood in the "Main Valley" transported by the Lena river during a flood. The position of the stem in the foreground of the image was measured with RTK GPS and had a height of 11 MASL. The location of the photograph is in about 30 m distance to TP 03 in the "Main Valley".

The influence of the warmer Lena water could be a reason for increased thawing of permafrost and thus the development of the extensive terrace structure in the "Main Valley" below 10 MASL. Flooding is not the main reason for their existence but could intensify their shape. The second identified terrace structure at about 10 MASL in profile TP 09 is an indicator of changing conditions during the evolution of the "Main Valley". The terrain surface in all observed profiles is at about 13 MASL and probably reflects the lower boundary of the Ice Complex deposits that formerly covered the area. *Schirrmeister et al.* [2011] detected the lower Ice Complex boundary between 15 and 20 MASL at the eastern coast of Kurungnakh Island, but the deposits could have been shifted in height due to tectonic uplift and the lower Ice Complex boundary could as well follow the general height gradient of Kurungnakh Island. Possibly several draining events of thermokarst lakes in the inland of Kurungnakh Island have initially led to the deep thermo-erosional incision in the "Main Valley" and the erosion of the Ice Complex in the area. Under the influence of floods by the Lena River the profiles were then smoothed and the extensive terrace structure formed.

The tributary with the profiles TP 01 and TP 02 shows an early stage of valley evolution in the transition of a diffuse surface channel to a v-shaped valley on a relatively short

distance. The other tributary described by the profiles TP 04 and TP 05 has a bigger catchment and is influenced by draining events more inland, connection to big alas north of the Lucky Lake. Their profiles are well developed and v-shaped and therefore show a high degree of erosional activity in the past.

In all of the observed valleys vegetation in the thalweg areas is much stronger and more active as in the adjacent not incised area, revealing increased water availability due to concentration of interflow from the terrain surface. Vegetation activity can be estimated through the strong signal of the near infrared channel of GeoEye-1 and RapidEye scenes (Figure 3-4). The valleys are therefore important spots for vegetation development and can feature very high growing vegetation compared to the usual Ice Complex surface. *Arp et al.* [2014] report that another form of combined thermokarst and thermal-erosion feature, called beaded river systems, which also occur in the study area play an important role in ecosystem functioning as summer feeding habitats and hydrologic connectivity for migrating fish.

6.4   Relevance of thermo-erosional features for arctic ecosystems

Three processes for future development of thermo-erosional features on Kurungnakh Island can be distinguished: 1) warming ice-rich permafrost is more sensible to degradation by thermo-erosional activity; 2) Lena River Delta channels will further erode the coasts of Kurungnakh Island with increasing intensity 3) and lateral expansion of thermokarst lakes and alasses due to thermo-erosional activity will take place (Figure 6-4).

Today's hydrological situation in the study area is particularly determined by the presence of ice-rich permafrost. Substantial changes of frozen ground and the cryosphere are reported in the Fifth Assessment Report of the Intergovernmental Panel on Climate Change (IPCC) by *Vaughan et al.* [2013], including decreasing snow cover extent, increasing permafrost temperatures, significant permafrost degradation and increased active layer thicknesses. These changes will consequently affect arctic stream networks. Warmer air temperatures and increased infiltration of precipitation leads to a deepening of the active layer and therefore the infiltration capacity of the soil is further increased [*Schuur et al.*, 2008]. This would consequently result in reduced surface runoff and decrease thermo-erosional activity. *Rowland et al.* [2010] again conclude that thermal erosion accompanied with permafrost thawing and the melting of ground ice will outweigh the storage effects of a deepened active layer. As *McNamara et al.* [1999] state, arctic drainage networks on hill slopes only have a rudimentary character, expressed as water tracks, and potential erosion is limited due to the presence of permafrost.
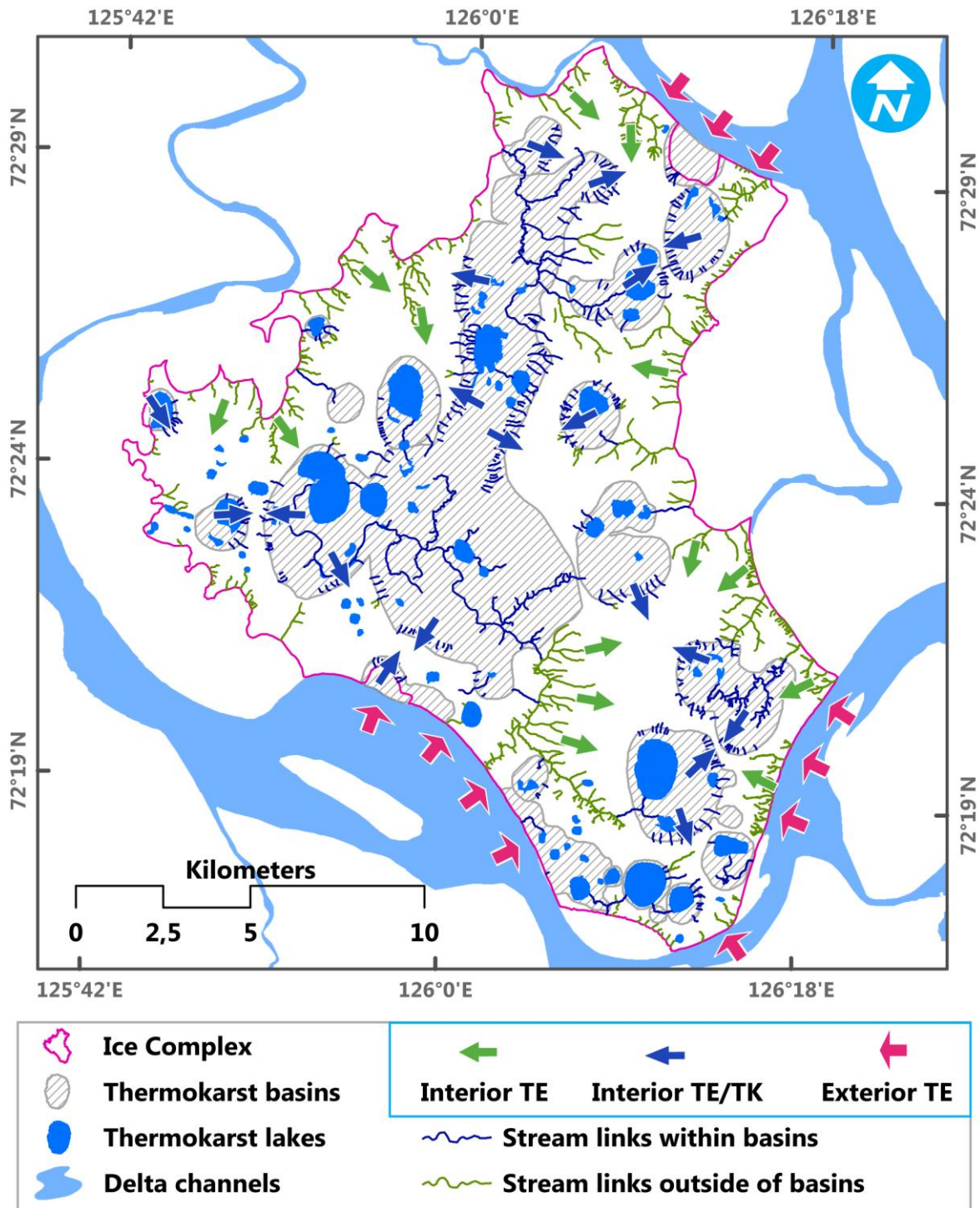
Figure 6-4: Scheme of main thermo-erosional processes on Kurungnakh and their future development. Red arrows show exterior thermo-erosional (TE) activity due to Lena River Delta channels, green arrows show interior thermo-erosional activity due to decreased stability of permafrost, blue arrows indicate lateral expansion of lakes and alasses due to combined thermo-erosional and thermokarst (TK) activity.

Under influence of rising temperatures in flowing surface water, permafrost is more sensible to degradation through thermo-erosion as laboratory experiments show [*Costard et al.*, 2007]. When the poorly developed stream networks on the Ice Complex can incise deeper into the permafrost it will form new and advanced networks. Increased draining of the adjacent surfaces will decrease their soil moisture contents, and therefore affecting land-

56

atmosphere moisture and energy fluxes, such as evaporative heat flux, and phase change in freezing or thawing of wet soil [*White et al.*, 2007].

While the formation of these new networks can occur in very short time [*Fortier et al.*, 2007], the resulting features are long lasting in periglacial landscapes and have a great impact on local hydrology, water availability for vegetation and therefore plant distribution as well as altering the sedimentary balance of river systems downstream due to ground loss following permafrost erosion [*Godin et al.*, 2014]. Accompanying with that carbon and nutrients from the organic-rich Ice Complex deposits will be mobilized and released to the Lena River Delta channels and to the Laptev Sea system, if they are not deposited in the watershed's floodplains or the wide alas valley floors. The amount of stream discharge following precipitation, snow melt or permafrost thawing is mainly regulating the intensity of the transport.

Concluding, the presence and future development of thermo-erosional valleys is of major importance for arctic ecosystems in the context of a warming climate. When accelerated degradation of permafrost and the accompanied reactivation of fossil organic carbon take place, thermo-erosional networks are the most important factor of transportation from the terrestrial place of degradation to the hydrosphere where exchange to the atmosphere or deposition in the near shore zone takes place. Future investigations about permafrost degradation and related sediment, nutrient and carbon fluxes should therefore incorporate thermokarst and thermal erosional processes, as well as their complex interrelationship.

7 Conclusions

The aim of this study was to morphometrically analyze thermo-erosional valleys in order to understand their distribution and dynamics within an arctic ice-rich permafrost site and to identify the main driving factors in the context of a warming arctic.

Photogrammetrically derived DEMs from high-resolution ALOS PRISM satellite images were successfully proven to be a valuable tool in lowland tundra landscapes, although low contrast and low height gradient limits the usability at wide and gentle alas slopes. The highest vertical accuracy of 4.41 MASL was achieved when using a combination of 6 stereopairs from 2006 and 2009. The DEM derived transversal and longitudinal profiles reflect the actual shape compared to the field data and mean slope values show mean deviations of 6.8° for 28 transversal and 0.5° for 3 longitudinal profiles.

Stream network analysis revealed that the majority (71%) of the detected stream links have a Strahler order of 1. These mostly short and straight streams are distributed heterogeneous in the study area and connect the Ice Complex surface with either the wide alas depressions inland or with the Lena River Delta channels. In the mostly poor developed stream network, the highest observed stream order of 4 was detected in three spots, of which 2 are located in a wide alas valley in the central part of the study area. The general orientation of the stream links follows the observed height gradient of the study area towards the northwest, but radially arranged short and straight streams at the slopes of thermokarst depressions superimpose the signal with directions towards east and west. Streams that are located outside of thermokarst basins showed two main directions towards northeast and northwest that could partly reflect the structure of polygonal nets in the ground.

Valley morphometries of three study sites were compared and differing driving factors for their evolution could be detected: V-shaped valleys incise deep into the Ice Complex and are driven by exterior thermal erosion due to the Lena Delta channels and or draining events within the study area or gullying due to rapid melting of ice wedges; U-shaped valleys with steep slopes and north to northwest facing terraces are influenced by snow patches, outflow of thermokarst lakes and in low areas by flooding of the delta channels; U-shaped and wide meandering valleys with gentle slopes and terraces that are also influenced by Lena River floods represent the most progressed state of valley evolution.

The lower barrier of the Ice Complex deposits possibly follows the height gradient of the study area. In contrast to the 15 to 20 MASL reported in the literature, a constant terrain surface height of 13 MASL in the westernmost highly degraded study site was observed. Based on this study, the development of semi-automated DEM classification approaches using morphometric parameters could help to identify the lower boundary of the Ice Complex

sequence when looking at characteristic slope changes in longitudinal and transversal cross profiles.

The results of this work show that thermo-erosional valley networks in Ice Complex landscapes of the Lena Delta are strongly connected to thermokarst activity. Changing permafrost conditions due to climate change will lead to an expansion of the thermo-erosional network and the close interaction of thermokarst and thermal erosion will increase the carbon, nutrient and sediment fluxes from the Ice Complex to the Laptev Sea system.

References

AMAP (2011), Snow, Water, Ice and Permafrost in the Arctic (SWIPA): Climate Change and the Cryosphere. Arctic Monitoring and Assessment Programme (AMAP)Rep., 538 pp, Oslo, Norway.

Are, F., and Reimnitz, E. (2000), An overview of the Lena River Delta setting: Geology, tectonics, geomorphology, and hydrology, *Journal of Coastal Research*, 16(4), 1083-1093.

Arp, C.D., Whitman, M.S., Jones, B.M., Grosse, G., Gaglioti, B.V., and Heim, K.C. (2014), Beaded streams of Arctic permafrost landscapes, *Biogeosciences Discuss.*, 11(7), 11391-11441.

Bignone, F., and Umakawa, H. (2008), Assessment of ALOS PRISM digital elevation model extraction over Japan, *The International Archives of the Photogrammetry, Remote Sensing and Spatial Information Sciences*, 37, 1135-1138.

Blackbridge (2013), Satellite Imagery Product SpecificationsRep.

Boike, J., et al. (2013), Baseline characteristics of climate, permafrost and land cover from a new permafrost observatory in the Lena River Delta, Siberia (1998-2011), *Biogeosciences*, 10(3), 2105-2128.

Brown, J., Ferrians, O.J., Heginbottom, J.A.J., and Melnikov, E.S. (1997), Circum-Arctic map of permafrost and ground-ice conditions., U.S. Geological Survey in Cooperation with the Circum-Pacific Council for Energy and Mineral Resources, Washington, DC.

Costard, F., Dupeyrat, L., Gautier, E., and Carey-Gailhardis, E. (2003), Fluvial thermal erosion investigations along a rapidly eroding river bank: Application to the Lena River (central Siberia), *Earth Surface Processes and Landforms*, 28(12), 1349-1359.

Costard, F., Gautier, E., Brunstein, D., Hammadi, J., Fedorov, A., Yang, D., and Dupeyrat, L. (2007), Impact of the global warming on the fluvial thermal erosion over the Lena river in Central Siberia, *Geophysical Research Letters*, 34(14).

Evans, I.S., and Minar, J. (2011), A classification of geomorphometric variables, paper presented at Geomorphometry, Redlands, California.

Fortier, D., Allard, M., and Shur, Y. (2007), Observation of rapid drainage system development by thermal erosion of ice wedges on Bylot island, Canadian Arctic Archipelago, *Permafrost and Periglacial Processes*, 18(3), 229-243.

Fraser, C.S., and Ravanbakhsh, M. (2009), Georeferencing Accuracy of GeoEye-1 Imagery, *Photogrammetric Engineering and Remote Sensing*, 75(6), 634-638.

French, H.M. (2007), *The Periglacial Environment*, Third ed., John Wiley and Sons Ltd, Chichester, UK.

Godin, E., Fortier, D., and Coulombe, S. (2014), Effects of thermo-erosion gullying on hydrologic flow networks, discharge and soil loss, *Environmental Research Letters*, 9(10), 105010.

Grigoriev, M.N. (1993), Cryomorphogenesis of the Lena River mouth area, Siberian Branch, in USSR Academy of Sciences, edited, p. 176, Yakutsk.

Grodecki, J., and Dial, G. (2003), Block adjustment of high-resolution satellite images described by rational polynomials, *Photogrammetric Engineering & Remote Sensing*, 69(1), 59-68.

Grosse, G., Schirrmeister, L., and Malthus, T.J. (2006), Application of Landsat-7 satellite data and a DEM for the quantification of thermokarst-affected terrain types in the periglacial Lena-Anabar coastal lowland, *Polar Research*, 25(1), 51-67.

Grosse, G., Schirrmeister, L., Siegert, C., Kunitsky, V.V., Slagoda, E.A., Andreev, A.A., and Dereviagyn, A.Y. (2007), Geological and geomorphological evolution of a sedimentary periglacial landscape in Northeast Siberia during the Late Quaternary, *Geomorphology*, 86(1-2), 25-51.

Gruen, A., and Wolff, K. (2007), DSM generation with ALOS/PRISM data using SAT-PP, paper presented at Geoscience and Remote Sensing Symposium, 2007. IGARSS 2007. IEEE International, 23-28 July 2007.

Günther, F. (2009), Untersuchung der Thermokarstentwicklung im südlichen Lena Delta anhand multitemporaler Fernerkundungs- und Felddaten, Diploma thesis, Technische Universität Dresden.

Günther, F., Overduin, P.P., Sandakov, A.V., Grosse, G., and Grigoriev, M.N. (2013), Short- and long-term thermo-erosion of ice-rich permafrost coasts in the Laptev Sea region, *Biogeosciences*, 10(6), 4297-4318.

Hasegawa, H., Matsuo, K., Koarai, M., Watanabe, N., Masaharu, H., and Fukushima, Y. (2000), DEM accuracy and the base to height (B/H) ratio of stereo images, *International Archives of Photogrammetry and Remote Sensing*, 33(B4/1; PART 4), 356-359.

Hauck, C. (2013), New Concepts in Geophysical Surveying and Data Interpretation for Permafrost Terrain, *Permafrost and Periglacial Processes*, 24(2), 131-137.

Heginbottom, J.A., Brown, J., Humlum, O., and Svensson, H. (2012), Permafrost and Periglacial Environments, in State of the Earth's Cryosphere at the Beginning of the 21st Century: Glaciers, Global Snow Cover, Floating Ice, and Permafrost and Periglacial Environments., edited by R. S. J. WILLIAMS and J. G. FERRIGNO, p. 78.

Holmes, R.M., et al. (2012), Seasonal and Annual Fluxes of Nutrients and Organic Matter from Large Rivers to the Arctic Ocean and Surrounding Seas, *Estuaries and Coasts*, 35(2), 369-382.

JAXA (2008), ALOS Data Users Handbook, edited, p. 158, Japan Aerospace Exploration Agency (JAXA), Earth Observation Research and Application Center (EORC).

Jones, B.M., Grosse, G., Arp, C.D., Jones, M.C., Anthony, K.M.W., and Romanovsky, V.E. (2011), Modern thermokarst lake dynamics in the continuous permafrost zone, northern Seward Peninsula, Alaska, *Journal of Geophysical Research-Biogeosciences*, 116.

Kääb, A. (2008), Remote sensing of permafrost-related problems and hazards, *Permafrost and Periglacial Processes*, 19(2), 107-136.

Kamiya, I. (2008), Reduction of JPEG Noise from the ALOS PRISM Products, *Bulletin of the Geographical Survey Institute*, 55, 31-38.

Koven, C.D., Ringeval, B., Friedlingstein, P., Ciais, P., Cadule, P., Khvorostyanov, D., Krinner, G., and Tarnocai, C. (2011), Permafrost carbon-climate feedbacks accelerate global warming, *Proceedings of the National Academy of Sciences*.

Kunitsky, V., Schirrmeister, L., Grosse, G., and Kienast, F. (2002), Snow patches in nival landscapes and their role for the Ice Complex formation in the Laptev Sea coastal lowlands, *Polarforschung*, 70, 53-67.

Kutzbach, L., Wagner, D., and Pfeiffer, E.-M. (2004), Effect of microrelief and vegetation on methane emission from wet polygonal tundra, Lena Delta, Northern Siberia, *Biogeochemistry*, 69(3), 341-362.

Lachenbruch, A.H. (1963), Contraction theroy of ice.wedge polygons: A qualitative ducussion, in Permafrost international conference, edited, National Academy of Scences-National Research Council, Lafayette.

Lantuit, H., Atkinson, D., Overduin, P.P., Grigoriev, M., Rachold, V., Grosse, G., and Hubberten, H.W. (2011), Coastal erosion dynamics on the permafrost-dominated Bykovsky Peninsula, north Siberia, 1951-2006, *Polar Research*, 30.

Lillesand, T.M., Kiefer, R.W., and Chipman, J.W. (2004), *Remote sensing and image interpretation*, John Wiley & Sons Ltd.

Mackay, J.R. (1972), The world of unerdground ice, *Annals of the Association of American Geographers*, 62(1), 1-22.

Mackay, J.R. (1990), Some observation on the growth and deformation of epigenetic, syngenetic and antisyngenetic ice wedges, *Permafrost and Periglacial Processes*, 1(1), 15-29.

McGuire, A.D., Anderson, L.G., Christensen, T.R., Dallimore, S., Guo, L.D., Hayes, D.J., Heimann, M., Lorenson, T.D., Macdonald, R.W., and Roulet, N. (2009), Sensitivity of the carbon cycle in the Arctic to climate change, *Ecological Monographs*, 79(4), 523-555.

McNamara, J.P., Kane, D.L., and Hinzman, L.D. (1999), An analysis of an arctic channel network using a digital elevation model, *Geomorphology*, 29(3–4), 339-353.

MDA, F. (2004), Landsat GeoCover ETM+ 2000 Edition Mosaics Tile N-52-70, USGS, Sioux Falls, South Dakota.

Mekik, C., and Arslanoglu, M. (2009), Investigation on accuracies of real time kinematic GPS for GIS applications, *Remote Sensing*, 1(1), 22-35.

Moigne, J.L., Netanyahu, N.S., and Eastman, R.D. (2011), *Image Registration for Remote Sensing*, Cambridge University Press.

Morgenstern, A. (2012), Thermokarst and thermal erosion: Degradation of Siberian ice-rich permafrost, Dissertation thesis, University of Potsdam.

Morgenstern, A., Grosse, G., Arcos, D.R., Günther, F., Overduin, P.P., and Schirrmeister, L. (2014), The role of thermal erosion oin the degradation of Siberian ice-rich permafrost, *Journal of Geophysical Research*, (under review).

Morgenstern, A., Grosse, G., Günther, F., Fedorova, I., and Schirrmeister, L. (2011), Spatial analyses of thermokarst lakes and basins in Yedoma landscapes of the Lena Delta, *Cryosphere*, 5(4), 849-867.

Morgenstern, A., Ulrich, M., Günther, F., Roessler, S., Fedorova, I.V., Rudaya, N.A., Wetterich, S., Boike, J., and Schirrmeister, L. (2013), Evolution of thermokarst in East Siberian ice-rich permafrost: A case study, *Geomorphology*, 201, 363-379.

PCI-Geomatics (2013), Geomatica 2013 - OrthoEngine User Guide, edited, p. 214.

Rachold, V., Grigoriev, M.N., Are, F.E., Solomon, S., Reimnitz, E., Kassens, H., and Antonow, M. (2000), Coastal erosion vs riverine sediment discharge in the Arctic Shelf seas, *International Journal of Earth Sciences*, 89(3), 450-460.

Raggam, H. (2006), Surface Mapping Using Image Triplets: Case Studies and Benefit Assessment in Comparison to Stereo Image Processing, *Photogrammetric Engineering & Remote Sensing*, 72(5), 551-563.

Ranalli, G., and Scheidegger, A.E. (1968), Topological significance of stream labeling methods, *Hydrological Sciences Journal*, 13(4), 77-85.

Romanovskii, N.N. (1977), Formirovaniye poligonal'nozhil'nykh struktur (Formation of polygonal-wedge structures), *Nauka*, 215.

Romanovskii, N.N., Hubberten, H.W., Gavrilov, A.V., Tumskoy, V.E., and Kholodov, A.L. (2004), Permafrost of the east Siberian Arctic shelf and coastal lowlands, *Quaternary Science Reviews*, 11, 1359-1369.

Romanovsky, V.E., et al. (2010a), Thermal state of permafrost in Russia, *Permafrost and Periglacial Processes*, 21(2), 136-155.

Romanovsky, V.E., Gruber, S., Instanes, A., Jin, H., Marchenko, S.S., Smith, S.L., Trombotto, D., and Walter, K.M. (2007), Frozen Ground (Chapter 7), in Global Outlook for Ice and Snow, edited, pp. 183-200, UNEP.

Romanovsky, V.E., Smith, S.L., and Christiansen, H.H. (2010b), Permafrost Thermal State in the Polar Northern Hemisphere during the International Polar Year 2007-2009: a Synthesis, *Permafrost and Periglacial Processes*, 21(2), 106-116.

Rowland, J.C., et al. (2010), Arctic Landscapes in Transition: Responses to Thawing Permafrost, *Eos, Transactions American Geophysical Union*, 91(26), 229-230.

Schirrmeister, L., Froese, D., Tumskoy, V., and Wetterich, S. (2012), Yedoma: Late Pleistocene ice-rich syngenetic permafrost of Beringia, *The Encyclopedia of Quaternary Science*, 542-552.

Schirrmeister, L., Kunitsky, V., Grosse, G., Wetterich, S., Meyer, H., Schwamborn, G., Babiy, O., Derevyagin, A., and Siegert, C. (2011), Sedimentary characteristics and origin of the Late Pleistocene Ice Complex on north-east Siberian Arctic coastal lowlands and islands – A review, *Quaternary international*, 241(1–2), 3-25.

Schuur, E.A.G., et al. (2008), Vulnerability of permafrost carbon to climate change: Implications for the global carbon cycle, *Bioscience*, 58(8), 701-714.

Schuur, E.A.G., Vogel, J.G., Crummer, K.G., Lee, H., Sickman, J.O., and Osterkamp, T.E. (2009), The effect of permafrost thaw on old carbon release and net carbon exchange from tundra, *Nature*, 459(7246), 556-559.

Schwamborn, G., Rachold, V., and Grigoriev, M.N. (2002), Late Quaternary Sedimentation History of the Lena Delta, *Quaternary international*, 89, 119-134.

Simone, G., Farina, A., Morabito, F.C., Serpico, S.B., and Bruzzone, L. (2002), Image fusion techniques for remote sensing applications, *Information Fusion*, 3(1), 3-15.

Soloviev, P.A. (1973), Thermokarst phenomena and landforms due to frost heaving in Central Yakutia, *Biuletyn Peryglacjalny*, 23, 135-155.

Stieglitz, M., Dery, S.J., Romanovsky, V.E., and Osterkamp, T.E. (2003), The role of snow cover in the warming of arctic permafrost, *Geophysical Research Letters*, 30(13).

Strahler, A.N. (1957), Quantitative analysis of watershed geomorphology, *Civ. Eng*, 101, 1258-1262.

Strauss, J. (2010), Late Quaternary environmental dynamics at the Duvanny Yar key section, Lower Kolyma, East Siberia, Diploma thesis, Universität Potsdam, Potsdam.

Takaku, J., Futamura, N., Iijima, T., Tadono, T., and Shimada, M. (2007), High resolution DSM generation from ALOS PRISM, paper presented at Geoscience and Remote Sensing Symposium, 2007. IGARSS 2007. IEEE International, 23-28 July 2007.

Tarnocai, C., Canadell, J.G., Schuur, E.A.G., Kuhry, P., Mazhitova, G., and Zimov, S. (2009), Soil organic carbon pools in the northern circumpolar permafrost region, *Global Biogeochemical Cycles*, 23(2), GB2023.

Tomirdiaro, S.V. (1982), Evolution of Lowland Landscapes in Northeastern Asia during Late Quaternary Time, in Paleoecology of Beringia, edited by D. M. Hopkins, J. V. Matthews, C. E. Schweger and S. B. Young, Academic Press, New York.

Toutin, T. (2004), Review article: Geometric processing of remote sensing images: models, algorithms and methods, *International Journal of Remote Sensing*, 25(10), 1893-1924.

Ulrich, M., Morgenstern, A., Gunther, F., Reiss, D., Bauch, K.E., Hauber, E., Rossler, S., and Schirrmeister, L. (2010), Thermokarst in Siberian ice-rich permafrost: Comparison to asymmetric scalloped depressions on Mars, *Journal of Geophysical Research-Planets*, 115.

van Everdingen, R. (2005), Multi-language glossary of permafrost and related ground-ice terms, edited by N. S. a. I. D. Center, Boulder, CO.

Vaughan, D.G., et al. (2013), Observations: Cryosphere, in Climate Change 2013: The Physical Science Basis. Contribution of Working Group I to the Fifth Assessment Report of the Intergovernmental Panel on Climate Change, edited by T. F. Stocker, D. Qin, G.-K. Plattner, M. Tignor, S. K. Allen, J. Boschung, A. Nauels, Y. Xia, V. Bex and P. M. Midgley, Cambridge University Press, Cambridge, United Kingdom and New York, NY, USA.

Walter, K.M., Zimov, S.A., Chanton, J.P., Verbyla, D., and Chapin, F.S. (2006), Methane bubbling from Siberian thaw lakes as a positive feedback to climate warming, *Nature*, 443(7107), 71-75.

Washburn, A.L. (1979), *Geocryology: A Survey of Periglacial Processes and Environments*, E. Arnold, London.

Weise, O.R. (1983), *Das Periglazial*, Gebrüder Borntraeger, Berlin, Stuttgart.

Wetterich, S., Kuzmina, S., Andreev, A.A., Kienast, F., Meyer, H., Schirrmeister, L., Kuznetsova, T., and Sierralta, M. (2008), Palaeoenvironmental dynamics inferred from late Quaternary permafrost deposits on Kurungnakh Island, Lena Delta, Northeast Siberia, Russia, *Quaternary Science Reviews*, 27(15-16), 1523-1540.

White, D., et al. (2007), The arctic freshwater system: Changes and impacts, *Journal of Geophysical Research-Biogeosciences*, 112(G4).

Wilson, J.P. (2012), Digital terrain modeling, *Geomorphology*, 137(1), 107-121.

Yun, Z. (2002), A new automatic approach for effectively fusing Landsat 7 as well as IKONOS images, paper presented at Geoscience and Remote Sensing Symposium, 2002. IGARSS '02. 2002 IEEE International, 24-28 June 2002.

Zhang, T., Barry, R.G., Knowles, K., Heginbottom, J.A., and Brown, J. (2008), Statistics and characteristics of permafrost and ground-ice distribution in the Northern Hemisphere, *Polar Geography*, 31(1-2), 47-68.

Zimov, S.A., Davydov, S.P., Zimova, G.M., Davydova, A.I., Schuur, E.A.G., Dutta, K., and Chapin, F.S. (2006), Permafrost carbon: Stock and decomposability of a globally significant carbon pool, *Geophysical Research Letters*, 33(20).

Danksagung

In besonderem Maße und an erster Stelle möchte ich mich bei Anne Morgenstern sowohl für die sehr gute Betreuung dieser Arbeit, als auch für die Förderung und das Vertrauen das mir entgegengebracht wurde herzlichst bedanken!

Einen herzlichen Dank auch an Herrn Prof. Dr. Tilman Rost für die Betreuung und Beratung seitens der Freien Universität Berlin.

Für eine tolle und intensive Teamarbeit mit unvergessenen sibirischen Erfahrungen während der Feldkampagne auf Samoylov und Kurungnakh, bedanke ich mich sehr herzlich bei Anne Morgenstern, Niko Bornemann, Sascha Nieman, Sonya Antonova und Antje Eulenburg!

Frank Günther möchte ich sowohl für seine wissenschaftliche und methodische Expertise in Form vieler konstruktiv kritischer Kommentare danken, die zu einer ständigen Reflektion der Arbeit beigetragen haben, als auch für eine sehr unterhaltsame Zeit als sein Büronachbar.

Ich danke allen Kolleginnen und Kollegen am AWI für den regen und interessanten Austausch und die stets gute Arbeitsatmosphäre. Besonderer Dank an Lutz Schirrmeister für das Interesse an meiner Arbeit und das Korrekturlesen. Paul Overduin und Fabian Kneier danke ich dafür, dass ich in den letzten Wochen einen phantastischen Arbeitsplatz nutzen konnte. Danke auch an Boris Radosavljevic für das Lösen mancher Knoten und an Juliane Wolter für manches Krisengelächter!

An alle meine Freunde, insbesondere meine Berliner Weggefährten der ersten Stunde, Manuel, Marcel, Kati, Dominik und Miriam geht ein großer Dank für ihre Unterstützung und die nötige Zerstreuung. Vielen Dank auch an Jack Mason für das Korrekturlesen.

Ein ganz großer Dank an Freund, Mitbewohner und Kollege George Tanski für einfach alles!

Für seine kenntnisreichen Beratungen in schweren Zeiten, welche mir immer außerordentlich viel bedeutet haben, danke ich ganz besonders meinem Bruder Simon.

Ewige Dankbarkeit möchte ich zuletzt für meine lieben und verständnisvollen Eltern zum Ausdruck bringen, die mich immer unterstützt und gefördert haben.

.

Selbständigkeitserklärung

Hiermit versichere ich, dass ich die vorliegende Arbeit selbstständig verfasst und keine anderen als die angegebenen Quellen und Hilfsmittel verwendet habe. Alle von Autoren wörtlich übernommenen Stellen, wie auch sich an die Gedanken anderer Autoren eng anlehnende Ausführungen meiner Arbeit, sind unter Angabe der Quelle kenntlich gemacht.

Berlin, den 27. November 2014

_____

Samuel Stettner